

# Where are the Fossils of the First Galaxies? II. True Fossils, Ghost Halos, and the Missing Bright Satellites

Mia S. Bovill and Massimo Ricotti

*Department of Astronomy, University of Maryland, College Park, MD 20740*

msbovill@astro.umd.edu

## ABSTRACT

We use a new set of cold dark matter simulations of the local universe to investigate the distribution of fossils of primordial dwarf galaxies within, and around the Milky Way. Throughout, we build upon previous results showing agreement between the observed stellar properties of a subset of the ultra-faint dwarfs and our simulated fossils. Here, we show that fossils of the first galaxies have galactocentric distributions and cumulative luminosity functions consistent with observations. In our model, we predict  $\sim 300$  luminous satellites orbiting the Milky Way, 50 – 70% of which are well preserved fossils. Within the Milky Way virial radius, the majority of these fossils have luminosities  $L_V < 10^5 L_\odot$ . Despite our multidimensional agreement with observations at low masses and luminosities the primordial model produces an overabundance of bright dwarf satellites ( $L_V > 10^4 L_\odot$ ) with respect to observations where observations are nearly complete. The “bright satellite problem” is most evident in the outer parts of the Milky Way. We estimate that, although relatively bright, the primordial stellar populations are very diffuse, producing a population with surface brightnesses below surveys detection limits and are easily stripped by tidal forces. Although we cannot yet present unmistakable evidence for the existence of the fossils of first galaxies in the Local Group, the results of our studies suggest observational strategies that may demonstrate their existence. i) The detection of “ghost halos” of primordial stars around isolated dwarfs would prove that stars formed in minihalos ( $M < 10^8 M_\odot$ ) before reionization, and strongly suggest that at least a fraction of the ultra-faint dwarfs are fossils of the first galaxies. ii) The existence of a yet unknown population of  $\sim 150$  Milky Way ultra-faints with half-light radii  $r_{hl} \approx 100 - 1000$  pc and luminosities  $L_V < 10^4 L_\odot$ , detectable by future deep surveys. These undetected dwarfs would have the mass-to-light ratios, stellar velocity dispersions and metallicities predicted in this work.

## 1. Introduction

Over the last decade, since Klypin et al. (1999) and Moore et al. (1999) showed that the number of dark matter subhalos expected around a Milky Way mass halo is two orders of magnitude above the number of known satellites, significant effort has been made in observation and theory to solve the substructure problem in cold dark matter (CDM) cosmology. Observational discoveries have redefined the ‘Missing

Galactic Satellite Problem’ with the number of observed Milky Way satellites now somewhat closer to theoretical expectations (Simon & Geha 2007; Tollerud et al. 2008; Bovill & Ricotti 2009; Macciò et al. 2010). The discovery of the ultra-faint dwarfs (Belokurov et al. 2006, 2007; Irwin et al. 2007; Walsh et al. 2007; Willman et al. 2005a,b; Zucker et al. 2006a,b; Geha et al. 2009) has roughly doubled the known Milky Way and M31 satellite populations since 2004. However, observations alone cannot fully explain the discrepancy between luminous satellites and CDM substructure.

One of the core theoretical issues of the “missing satellites” problem remains the relationship between luminosity of satellites and the virial mass at formation of their dark matter halos. From a theoretical perspective, the fundamental question to be answered is: “What is the minimum halo mass which can host a luminous galaxy?” Previous studies (Efstathiou 1992; Thoul & Weinberg 1996; Bullock et al. 2001; Venkatesan et al. 2001; Ricotti & Ostriker 2004; Ricotti et al. 2005) have shown that this critical mass is set by the reheating history of the intergalactic medium (IGM) (Ricotti et al. 2000) and by feedback loops operating before reionization which determine whether low mass minihalos with  $M < 10^8 M_\odot$  are able to accrete gas from the IGM and form stars. Simulations show that for halos with masses  $M < 10^8 M_\odot$  the local and stochastic components of galaxy feedback produce minihalos with the same dark matter mass, but with stellar masses which vary by several orders of magnitude (Ricotti et al. 2008). It is likely unjustified to assume a sharp mass threshold separating dark and luminous halos and/or a tight relationship between dwarfs’ luminosities and their total mass, at the faint end of the luminosity function. This is one of the main motivations for the present study.

Cooling in halos with masses at formation,  $M > 10^8 M_\odot$  ( $v_{max} > 20$  km/s) is initiated via readily available hydrogen Lyman- $\alpha$  emission. However, cooling in minihalos with  $T_{vir} < 10^4$  K requires the formation of either molecular hydrogen or pre-enrichment with metals from nearby galaxies. The balance between the destruction and formation of  $H_2$  and metal transport in the IGM governs whether or not low mass minihalos can initiate cooling and form stars. If ultraviolet  $H_2$  dissociating radiation dominates, star formation in the first minihalos may be suppressed or delayed (Haiman et al. 2000; Ciardi et al. 2000; Machacek et al. 2000; Wise & Abel 2007; O’Shea & Norman 2008; Maio et al. 2010). However, if ionizing ultraviolet radiation ( $h\nu > 13.6$  eV) is the dominant feedback mechanism,  $H_2$  formation can be catalyzed inside relic HII regions and on the edges of Stromegen spheres (Ricotti et al. 2001, 2002a,b; Ahn et al. 2006; Whalen et al. 2008; Wise & Abel 2008), allowing star formation to be more widespread in minihalos with mass  $M \lesssim 10^8 M_\odot$ , before reionization. It is important to emphasize that, regardless of the interplay between the creation and destruction of  $H_2$ , not every minihalo will host a galaxy.

The ultra-faint dwarfs are an excellent laboratory for testing models of star formation in the lowest mass halos, due to their extremely low luminosities:  $10^2 - 10^5 L_\odot$ , low dynamical masses:  $M \lesssim 10^7 M_\odot$  (Strigari et al. 2008; Walker et al. 2010; Wolf et al. 2010), and their estimated large number (Koposov et al. 2008; Tollerud et al. 2008; Walsh et al. 2009). In Bovill & Ricotti (2009) and Bovill & Ricotti (2010a) (hereafter Paper I), we argue that the properties of the ultra-faint dwarfs are consistent with those of simulated primordial fossil galaxies. Kravtsov (2010) has argued that the missing galactic satellites can be accounted for by a simple model in which the fraction of baryons turned into stars,  $f_*$  decreases with the virial mass in a halo before its infall into a Milky Way. Not surprisingly, our simulations of pre-reionization dwarf galaxies

naturally produce such a decrease of star formation efficiency with mass, although with increasing scatter at small masses (Ricotti et al. 2008).

Assuming the observed ultra-faints belong to an isotropically distributed satellite population around the Milky Way (but see, Metz et al. 2007, 2009; Bailin et al. 2008), one infers from observations a minimum of 60-65 satellites within 200 kpc of the Galactic center. This number is consistent with all the satellites being subhalos that formed after reionization. There are about 90 (60) subhalos that during their evolution had a maximum circular velocity above 20 km/s (30 km/s), thus likely formed most of their stars after reionization (Bovill & Ricotti 2009) (hereafter BR09). However, we know that most satellites with  $L_V < 10^4 L_\odot$  are undetectable beyond 50–100 kpc (Simon & Geha 2007). Once luminosity corrections are folded into estimates of the satellite counts, the number of satellites inferred from observations is  $\sim 200 - 250$  (Tollerud et al. 2008; Walsh et al. 2009), suggesting that around the Milky Way there could be  $\sim 100 - 150$  true pre-reionization fossils (for a review see, Ricotti 2010). Nevertheless, these luminosity corrections are uncertain and model dependent, hence it is largely unknown how many ultra-faints may exist in the outer parts of the Milky Way. Indeed, the dimmest ultra-faint dwarfs within 50 kpc of the Milky Way may belong to a different population: according to our simulations, they have properties that are inconsistent with well preserved fossils, suggesting that may have been shaped by tidal forces. Some observations also seem to reinforce this hypothesis (McGaugh & Wolf 2010; Willman et al. 2010; Sand et al. 2009; Frebel et al. 2010). In summary, although there is circumstantial evidence that a fraction of the new ultra-faint dwarfs represent a well preserved primordial population in halos with infall masses corresponding to  $v_{max} \lesssim 20 - 30 \text{ km s}^{-2}$ , we have yet to find observational proof of their existence.

But is this “primordial scenario” consistent with observations when we move beyond the virial radius of our own galaxy and peer into the voids? Unless the local component of galaxy feedback is very strong, star formation should proceed similarly in small mass halos regardless of a halo’s location relative to the Local Group. Therefore, the voids should be populated with luminous objects (see Figure 1 of Paper I). As first noted in Peebles (2001), they are not. The number of dwarf galaxies with absolute magnitude  $M_V > -16$  ( $L_V < 2 \times 10^8 L_\odot$ ) observed in the voids is smaller than expected in CDM cosmologies (Karachentsev et al. 2004, 2006; Tully et al. 2006). According to Tikhonov & Klypin (2009), the luminosity function can only be reconciled if halos with  $v_{max} < 35 \text{ km s}^{-1}$  are dark. However, such a large mass threshold for star formation would produce less than 35 luminous satellites between 100-200 kpc of the Milky Way. That is inconsistent with observations unless satellites with  $L_V < 10^4 L_\odot$  do not exist beyond 100 kpc (see Figs. 3-4 in this paper).

Alternatively, if the star formation rate is primarily determined by halo mass, the void phenomenon can be reconciled with CDM by using a halo occupation distribution for which the  $M/L$  ratio increases with decreasing halo mass. However, this solution has only been tested for halos with  $M > 10^{10} M_\odot$  (Tinker & Conroy 2009), three orders of magnitude more massive than our fossils. When we extend their  $M/L \sim M^{-1}$  relation to our mass range we obtain a  $M/L$  ratio  $\gtrsim 10^5$  for the fossil population ( $M \lesssim 10^8 M_\odot$ ). This would produce an “ultra-faint” population with  $M/L$  ratios  $\sim 2 - 3$  orders of magnitude greater than those seen for the primordial fossils in Ricotti et al. (2002b)

In this paper, we investigate the following conundrum: can we simultaneously account for the predicted and observed subhalo population around the Milky Way and the lack of isolated galaxies with  $M_V > -16$  in the voids? Is a primordial origin scenario for ultra-faint dwarfs, consistent with the number of dwarfs in the voids? The simulations described in Paper I allow us to address both of these populations within the same theoretical framework. As a result of this study, we will propose three new observational strategies to search for evidence of fossil galaxies in the local universe. We will argue that, if stars formed in halos with masses  $M < 10^8 M_\odot$  there should be diffuse “ghost halos” of primordial stars around isolated dwarfs, in addition to the undetected population of lower surface brightness ultra-faint dwarfs.

This paper is structured as follows. § 2 and 3 summarize the numerical method and treatment of the observations, covered in detail in Paper I. In § 4 we discuss the radial distribution of the fossils of the first galaxies and make comparisons to other N-body simulations (§ 4.1) and we show agreement between the radial distributions and cumulative luminosity functions of primordial fossils in our simulations and the observed ultra-faint satellites (§ 4.2). We also discuss a possible origin of Willman I type ultra-faint dwarfs and the exception of Segue I. In § 5, we describe an overabundance of bright satellites in the outer parts of the Milky Way halo and investigate possible solutions. In § 6, we propose observational tests for our models. Discussion and a summary are presented in § 7.

## 2. Numerical Method

In this paper, we continue our analysis of the simulations described in Paper I. In brief, we used a set of hybrid initial conditions for a  $\Lambda$ CDM N-body simulation to give us the resolution necessary to study the primordial fossils on Local Volume scales. Our high resolution region, centered on a ‘Local Group,’ is generated as follows. Instead of using a uniform grid of particles, on scales  $l < 1$  Mpc, the positions and velocities of our halos are set by the final outputs of the Ricotti et al. (2002a,b, 2008) simulations, hereafter referred to as the pre-reionization simulations. Perturbations on scales  $l > 1$  Mpc are added to the initial positions and velocities of particles at  $z = z_{init}$  using a coarse resolution simulation run from  $z = 40$  to  $z = 0$ . For more detail, we direct the reader to the appendix of Paper I. In addition to the non-uniform initial grid of particles, the particles in the high resolution region have masses set by the mass function of the final pre-reionization outputs. Thus, we do not need to resolve these pre-reionization halos, just trace their merger history, tidal disruption, and positions from reionization to present day.

Paper I details the two realizations of our initial conditions. Our first order realization (see Appendix in Paper I for details) uses the same pre-reionization output across the entire high resolution region, and consequently does not account for the slower rate of structure evolution in the voids. In contrast, our second order initial conditions use four outputs from the pre-reionization simulations and do account for slower rate of structure formation in the voids (Barkana & Loeb 2004). Near the Milky Way, where this paper is concerned, we find no substantive difference between the two realizations. We therefore focus our discussion on the second order initial conditions.

All the simulations discussed in this paper were run using Gadget 2 (Springel 2005) and analyzed

using the halo finder AHF (Knollmann & Knebe 2009). Simulation and data analysis were run on the beowulf cluster Deepthought at the HPCC at the University of Maryland. At  $z = 0$  we define a bound halo as anything identified by AHF that, for the parameters we used, produces mass functions complete for halos with a number of particles  $N > 50$ . Paper I shows that our hybrid initial conditions and non-uniform particle masses produce results consistent with traditional CDM N-body simulations on both Local Volume and galactic subhalo scales. The parameters of the three ‘Milky Ways’ contained within our two highest resolution runs are listed in Table 1.

### 2.1. Fossil Definition

Dark matter halos identified in our simulations at  $z = 0$  are divided into three populations based on their ability to accrete gas from the IGM and form stars after reionization. A just virialized halo is able to accrete gas after reionization only if its maximum circular velocity,  $v_{max}$ , is larger than a filtering velocity,  $v_{filt}$ . In this work, we use  $v_{filt} = 20 - 30 \text{ km s}^{-1}$ , corresponding to the threshold for cooling via Lyman- $\alpha$ . Paper I and GK06 show that the exact choice of the filtering velocity does not significantly change the results. If a  $z = 0$  halo has  $v_{max} > v_{filt}$ , we classify it as a *non-fossil*. In the modern epoch, non-fossils can be identified as dIrrs which have been accreting gas and forming stars continuously since reionization.

Any halos whose present day  $v_{max}$  is below the filtering velocity is a *candidate fossil*. A candidate fossil for which  $v_{max} > v_{filt}$  at any point during its evolution may have accreted gas and/or formed stars after reionization. We include them in the “non-fossil” group, as post-reionization stars may be the dominant stellar population. When we need to distinguish these “candidate fossils” from the broader “non-fossil” group, we will refer to them as *polluted fossils*. Finally, any candidate fossil for which  $v_{max} < v_{filt}$  from reionization to the modern epoch is a *true fossil*. True fossils formed the majority ( $> 70\%$ ) of their stars before reionization and today would be relatively diffuse systems of old stars devoid of gas (Ricotti & Gnedin 2005). The term *fossil* will only refer to “true fossils”. Unless otherwise specified, the term non-fossil will apply to any halo which could have accreted gas after reionization regardless of its maximum circular velocity at  $z = 0$ .

The division of the Milky Way and M31 satellites into fossils and non-fossils is shown in Table 2. We

Table 1. Table of ‘Milky Ways’

| Name | Run | Mass<br>( $10^{12} M_{\odot}$ ) | $R_{vir}$<br>(kpc) | $v_{max}$<br>( $\text{km s}^{-1}$ ) |
|------|-----|---------------------------------|--------------------|-------------------------------------|
| MW.1 | C   | 1.82                            | 248                | 203                                 |
| MW.2 | D   | 0.87                            | 222                | 196                                 |
| MW.3 | D   | 1.32                            | 194                | 177                                 |

distinguish between the seven, classical RG05 fossils above the  $10^6 L_{\odot}$  threshold, the RG05 fossils with  $L_V < 10^6 L_{\odot}$  and the ultra-faint dwarfs discovered since 2005.

### 3. A Note on Observations

We approach the observations as follows. The majority of the information on the classical dwarfs comes from the Mateo (1998) review. For the ultra-faint dwarfs we generally defer to measurements with the smallest error bars with some weight given to more recent work (Walker et al. (2009)). We direct the reader to Paper I of this series and BR09 for a more complete discussion of these criteria.

When calculating the observed distributions of dwarfs around the Milky Way, we account for two effects, the sky coverage of the SDSS, and its detection efficiencies (Walsh et al. 2009; Koposov et al. 2008). For the classical dwarfs, we assume the entire sky has been covered and only apply sky coverage corrections to the ultra-faint population. To correct for the SDSS sky coverage, we assume that the satellite distribution around the Milky Way is isotropic, and multiply the number of ultra-faints by 3.54 to account for the nearly three-quarters of the sky not surveyed by SDSS, now past Data Release 7 (Abazajian et al. 2009). However, bright satellites of the Milky Way are distributed very anisotropically (Kroupa et al. 2005; Zentner et al. 2005; Metz et al. 2007, 2009; Bozek et al. 2011), so the assumption of isotropy may not be a good one.

Next, we apply a correction for the detection efficiency of the SDSS using the results from Walsh et al. (2009). If an ultra-faint is bright enough to be detected with 99% efficiency, we assume the sample is complete for that luminosity and distance. However, if the ultra-faint is too dim for 99% detection, but bright enough to be detected half the time, we assume that, statistically, there is another satellite with similar luminosity and distance missed by SDSS. This second correction produces only a minor increase in the number of satellites; approximately one additional satellite over a total of  $\sim 60$  from sky coverage correction alone.

As discussed in Section 4 of Paper I, we also divide the ultra-faint dwarfs into two groups. The first is a group of seven, including CVnI and II, Hercules, Leo IV, Leo T, and Ursa Major I and II, have half light radii and surface brightnesses which are consistent with the stellar properties of fossils of the first galaxies. In contrast, the second group composed of five members, including Willman 1, Segue 1 and 2, Leo V, and Pisces II, have half light radii which are too small, and surface brightnesses which are too high, to be consistent with the simulated primordial population.

Table 3 shows the Milky Way ultra-faint dwarfs classified in two ways, (i) the satellites within and beyond 50 kpc, and (ii) those which are consistent (opened circles in right panel of Figure 11 of BR11a) and those which are inconsistent (filled green circles in the same figure) with the expected properties of fossil dwarfs. Excepting Leo V and Pisces II, the dwarfs which have half-light radii significantly smaller than the simulations are also within 50 kpc of the Milky Way. Conversely, all the ultra-faint dwarfs which are consistent with the simulations are beyond 50 kpc, except Coma Ber.. In this paper, we will refer to this second population collectively as the “inner ultra-faints,” to emphasize their location within the Local Group.

|           | Non-fossils  | Fossils   |  |   |
|-----------|--|---|--|---|
|           |  | RG05 only   | RG05 & BR11a   | BR11a only  |
| Milky Way | LMC<br>NGC 55<br>Sextans A & B<br>SMC<br>WLM<br><i>Carina</i><br><i>Fornax</i><br><i>GR8</i><br><i>Leo I, II &amp; A</i><br><i>Sagittarius</i> | Sculptor  | Draco <sup>1</sup><br>Phoenix<br>Sextans<br>Ursa Minor | Bootes I & II<br>CVn I & II<br>Hercules<br>Leo IV & T <sup>2</sup><br>Pisces II   |
| M31       | IC 10<br>IC 1613<br>IC 5152<br>M32<br>NGC 185<br>NGC 205<br>NGC 3109<br>NGC 6822<br><i>DDO 210</i><br><i>LGC3</i><br><i>Pegasus</i>            | And I & II<br>And III<br>And VI<br>Antila<br>KKR 25 | And V  | And XI XII<br>And XIII & IV<br>And XV & XVI<br>And XVII & XVIII<br>And XX & And XXI<br>And XXII & XXIII<br>And XXIV & XXV<br>And XXVI & XXVII |
| Isolated  | —  | —   | Cetus <sup>3</sup><br>Tucana                           | —   |

Table 2: Table of all the Local Group dwarfs divided by their host (or lack there of) and their non-fossil or fossil status. We have further divided the fossils into three groups, those considered fossils in RG05, but with  $L_V > 10^6 L_\odot$ , the “classical” fossil dwarfs with luminosities below the  $10^6 L_\odot$  threshold from BR11a, and, finally, those satellites which were only included in BR11a,b due to their post-2004 discovery. Three of dwarf initially identified as fossils show interesting properties (1) a small fraction of the stars in Draco are of intermediate age (Cioni & Habing 2005), (2) Leo T has  $\sim 10^5 M_\odot$  of gas and a young stellar population (de Jong et al. 2008), and (3) Cetus shows evidence for star formation through  $z \sim 1$  (Monelli et al. 2010).

Though we are agnostic about its status, Segue 1 may be an exception. Recent work (Simon et al. 2010; Martinez et al. 2010) suggest that its stellar population has remained well within its tidal radius (thus tides are not important) and its stars are unaffected by interactions with the Milky Way. However, other work suggests that Segue 1 is a highly disrupted star cluster or dwarf (Niederste-Ostholt et al. 2009; Norris et al. 2010). We note that, *if* Segue 1 is an undisrupted dwarf, the high concentration which has protected Segue 1’s stars also identifies it as a rare object formed in a high sigma peak at high redshift. The  $1 \text{ Mpc}^3$  volume of our pre-reionization simulations does not represent a large enough volume to contain a Segue 1. If Segue 1 is an undisrupted dwarf, then yes, if there are more than one or two additional Segue 1 like objects in the Milky Way halo it is a problem for our model that produces larger half-light radii than Segue 1’s. However, if Segue 1 is disrupting then (i) we would not expect to see objects of that type beyond 100 kpc from the Milky Way, and (ii) the presence of additional Segue 1 objects would not pose a problem.

The ultra-faint dwarfs in the first group, and the classical dSph noted in Ricotti & Gnedin (2005) are the best candidates for an observed population of primordial fossils, with stellar spheroids not significantly modified by tides. However, as noted in Paper I, classical dwarfs with  $L_V > 10^6 L_\odot$  are too bright to be hosted in halos with  $v_{max} < v_{filt}$  for  $v_{filt} = 20 \text{ km s}^{-1}$  or  $30 \text{ km s}^{-1}$ . While they may have formed most of their stars before reionization, we exclude them from our comparison to be as conservative as possible.

Throughout this work, and in Paper I, we compare the observed Milky Way satellites to our luminous  $z = 0$  halos with  $\Sigma_V > 10^{-1.4} L_\odot \text{ pc}^{-2}$ . We are also able to use our simulations to study the distribution of a hereto undetected population of ultra-faints with  $\Sigma_V < 10^{-1.4} L_\odot \text{ pc}^{-2}$  and  $L_V \lesssim 10^4 L_\odot$ . The possible existence and undetectability of this population was first noticed in BR09, from the analysis of RG05 simulations (see also Ricotti 2010 for a review). However, using independent arguments, Bullock et al. (2010) have also proposed the existence of this population they refer to as “stealth galaxies.”

## 4. Results

In this section, we compare the distributions of non-fossils and true-fossils to the galactocentric radial distribution of the observed Milky Way satellites. We first compare the galactocentric radial distributions of our simulations to observations. We then make detailed comparisons between the observed cumulative luminosity function of the Milky Way satellites and the simulated cumulative luminosity functions of our non-fossil and true fossil populations. Note, that our simulated cumulative luminosity functions only include stellar populations formed before reionization. Therefore, we refer to our simulated cumulative luminosity functions as primordial cumulative luminosity functions. Any star formation that may take place in halos with  $v_{max} > v_{filt}$  after reionization is not accounted for in our simulated luminosity functions. Thus, only the cumulative luminosity function of true fossils can be directly compared to observations, while the luminosities of the non-fossils are lower limits.



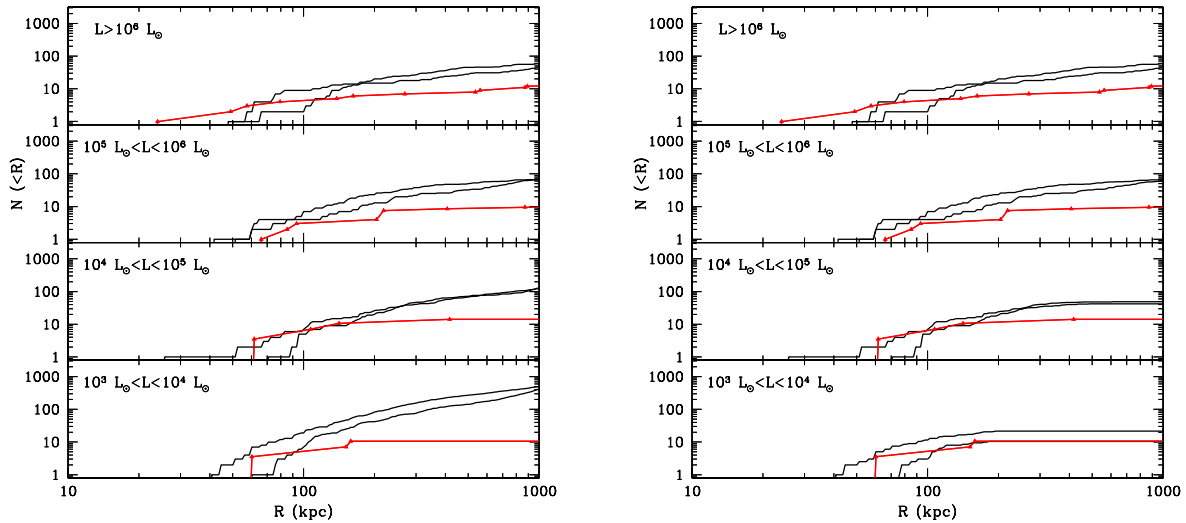


Fig. 1.— *Left* Galactocentric radial distribution of all simulated satellites for MW.2 and MW.3 from Run D (black curves) compared to the radial distribution of all observed Milky Way satellites (red triangles). We have included all simulated subhalos and known satellites regardless of their classification or whether they are detectable. *Right* Same as the left panel but we have convolved our populations with Walsh et al. (2009) detection limits and only included simulated subhalos which can be detected in the SDSS data.

#### 4.1. Radial Distribution of Fossils Near Milky Ways

Figure 1 shows the galactocentric radial distribution of all the simulated and observed Milky Way satellites. In the left panel of Figure 1, we compare observations to simulations without correcting for the sensitivity limits of the SDSS (Walsh et al. 2009; Koposov et al. 2008) or whether a satellite is a fossil. In the right panel, we show all the satellites again, now applying the Walsh et al. (2009) limits to the simulated halos around MW.2 and MW.3. Figure 2 shows the galactocentric radial distribution for only the observed and simulated *fossils*. As in Figure 1, the right and left panels show the simulated true fossils with and without the Walsh et al. (2009) corrections. The observational and theoretical fossil definitions are discussed in Sections 3 and 2.1, respectively. Our simulations do not account for tidal stripping of stars, and do not reproduce the properties of the inner ultra-faint dwarfs, and we do not include them in Figure 2.

The left panels of Figures 1 and 2 show that at  $L_V \sim 10^5 L_\odot$  the fossils become a significant fraction of the satellite population, with fossil dominance increasing as satellite luminosity decreases. This is further illustrated in Figure 4, which shows the fraction of subhalos which are fossils,  $N_{fos}/N_{all}$ , as a function of distance from the host for the same luminosity bins as Figure 2, excepting  $L_V > 10^6 L_\odot$ . We find that for  $10^5 L_\odot < L_V < 10^6 L_\odot$  bin, the fraction of fossils is 0.05-0.1, with the fraction decreasing as host halo mass increases. For the lower luminosity bins,  $N_{fos}/N_{all}$  converges to 40 – 50% and 70 – 80% for  $10^4 - 10^5 L_\odot$  and  $10^3 - 10^4 L_\odot$  bins, respectively. If we include the inner ultra-faints in our galactocentric radial distributions, we find a significant overabundance of observed dwarfs within 50 kpc of the Milky Way.

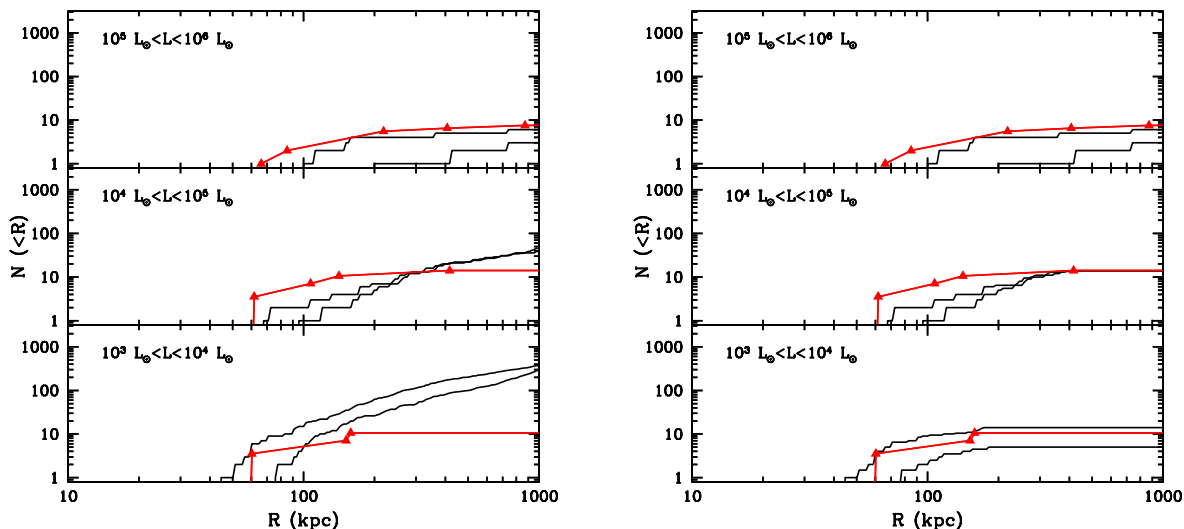


Fig. 2.— *Left* Same as Fig. 1 but the observed satellite distributions only include bona fide fossils: the classical dSph which were designated fossils in Ricotti & Gnedin (2005) and the ultra-faints whose stellar properties match those of the simulated fossil population. Note that this excludes most of the ultra-faints within 50 kpc. In our simulated distributions we use  $v_{filter} = 20 \text{ km s}^{-1}$  to define a fossil. We have included all simulated fossils, including those which would sit below the SDSS detection limits. *Right* Same as the left panel but simulated radial distributions only include the true fossils which would fall within the Walsh et al. (2009) detection limits.

The stellar properties of the inner ultra-faint dwarfs do not agree with the simulated stellar properties of the fossils. As discussed in Paper I, and § 3 of this work, we argue the majority of these objects may represent a population of tidally stripped remnants of once more luminous dwarfs. A possible exception, Segue 1, is discussed in § 3. Our simulations are also unable to reliably resolve  $z = 0$  halos within 50 kpc of the Milky Way. We therefore have excluded anything with  $R < 50$  kpc from our comparisons.

Without the ultra-faints with  $R < 50$  kpc, the right panels of Figures 1 and 2 show good agreement between the simulated satellite distributions of the true fossils around MW.2 and MW.3 and the observed Milky Way galactocentric radial distribution. When we convolve our simulated satellite populations with the limits from Walsh et al. (2009), we find that the agreement between the distribution of dwarfs around MW.2 and MW.3 and that observed around the Milky Way agree at all radii and luminosity bins for  $L_V < 10^6 L_\odot$  (see right panel of Figure 2). We thus argue that, in addition to matching the stellar properties of the ultra-faints, our simulated fossils also agree with their galactocentric radial distribution.

Figure 3 shows the galactocentric radial distribution of the *undetected* fossils in our simulations, after excluding detectable fossils according to the detection criterion from Walsh et al. (2009). We have not included the bins with  $L_V > 10^5 L_\odot$  because there are no undetected fossils in this luminosity range within 1 Mpc of the Milky Way. In addition, all fossils with  $L_V > 10^4 L_\odot$  are detected within 200 kpc. For

the lowest luminosity fossils ( $L_V < 10^4 L_\odot$ ) we find  $\sim 400 - 500$  undetected dwarfs within 1 Mpc and 150 within 200 kpc. We have included a panel for very low luminosity bin ( $10^2 - 10^3 L_\odot$ ) to look at the distribution of the dimmest fossils which are invisible beyond a few tens of kpc. While the shape of the distribution in the lowest luminosity bins is similar there are approximately two times fewer undetected fossils in the  $10^2 - 10^3 L_\odot$  bin. Given that *fewer* of the fossils in this bin would be detected compared to its higher luminosity counterpart, we are seeing the decline of star formation in the minihalos with the lowest mass. There are simply fewer  $10^2 - 10^3 L_\odot$  pre-reionization fossils around the Milky Way than their  $10^3 - 10^4 L_\odot$  counterparts.

On the other end of the luminosity spectrum, the right panel of Figure 1 shows that while our simulated fossils are able to reproduce the ultra-faint distribution, we see too many massive, bright ( $L_V > 10^4 L_\odot$ ) satellites at  $R > R_{vir}$ , even after the Walsh et al. (2009) corrections are applied. We note that this discrepancy does not exist in the lowest,  $10^3 - 10^4 L_\odot$  luminosity bin. This is the first evidence of an apparent discrepancy between simulations and observations we refer to as the “bright satellite problem.” In the next sections, we will analyze this discrepancy, try to understand its origin, and whether it can be removed while maintaining the agreement of the simulations with observations at smaller radii and lower luminosities.

#### 4.2. Primordial Cumulative Luminosity Functions

We next explore the fossil distribution and “bright satellite problem” from another angle via comparisons between simulated cumulative primordial luminosity functions and the observed cumulative luminosity function at different galactocentric distances from the Milky Way center. Results are equivalent for all three simulated Milky Ways and for both versions of our initial conditions. Therefore, for the remainder of this section and the next we will be discussing the results for MW.3 in Run D.

Each cumulative luminosity function in this paper is split into four radial bins to probe different regimes. We choose not to include the sample at  $R < 50$  kpc, where the observational sample is the most complete, because tidal effects are prevalent and our simulations do not have sufficient resolution to determine whether or not pre-reionization halos stripped of their enveloping cloud of tracer particles have been tidally disrupted. The first bin we consider shows  $50 \text{ kpc} < R < 100 \text{ kpc}$ . The next bin out, the outer portion of the Milky Way halo from 100 kpc to 200 kpc, has observations which are fairly complete for  $L_V > 10^4 L_\odot$ , including the brightest ultra-faints. From 200 kpc to 500 kpc all but two of the ultra-faints (CVnI and Leo T) would be below the detection limits of the surveys and would not be visible. Roughly, this region corresponds to the virial radius ( $R_{200} \sim 200 \text{ kpc}$ ) to  $R_{50}$  for a Milky Way mass halo. Specific to our Local Group, this is the regime where M31 begins to play a significant role in the satellite counts, increasing the care required to separate the Milky Way and Local Group dwarfs from those bound to M31. The final radial bin, from 500 kpc to 1 Mpc, probes the transition region from the edge of the Milky Way halo to the surrounding filament and void. Subhalos at these radii are just beginning to fall into the host system, and all the ultra-faints are below detection limits.

We divide the simulated satellites into fossils and non-fossils: Figure 5 shows the primordial cumulative

luminosity functions in the four radial bins for fossil thresholds  $v_{filt} = 20$  km/s (left panel) and  $v_{filt} = 30$  km/s (right panel). The observed cumulative luminosity function is shown as magenta lines and includes all the classical dwarfs and the ultra-faints, excepting the population at  $R < 50$  kpc. The simulated non-fossils are shown as the red solid curve, and for all bins they dominate for  $L_V > 10^4 - 10^5 L_\odot$ . These halos may have been able to accrete gas and form stars after reionization, and their primordial cumulative luminosities represent a lower limit for their present day luminosity. If we were to allow for additional star formation after reionization, the total number of luminous non-fossils would remain constant, but the curve would shift to higher luminosities (to the right). The primordial cumulative luminosity function of the true fossils (blue dashed curve) has no such caveat. Their luminosities are known since they have not undergone post-reionization baryonic evolution aside from the aging of their stellar populations. The primordial cumulative luminosity function of the entire simulated population is the solid black curve. Note, that for  $L_V < 10^5 L_\odot$ , the total primordial cumulative luminosity function is increasingly dominated by fossils.

Before looking at the primordial cumulative luminosity functions in detail, we insure we are comparing equivalent populations. By definition, all observed Milky Way satellites are above current detection limits, however, as seen in Paper I, a subset of our simulated fossils have surface brightnesses below the detection limit of the SDSS. We use both the Walsh et al. (2009) and Koposov et al. (2008) limits to test the distribution of detectable true fossils against observations. Figure 6 shows the true fossil luminosity function convolved with the Walsh et al. (2009) limits (blue dashed line) and the observed fossil sample (magenta line) used in Figure 2. As in the galactocentric radial distributions, we find good agreement between the primordial luminosity function of the true fossils and the observed fossils for 50 – 100 kpc and 100 – 200 kpc. We do not make comparisons at  $R > 200$  kpc because of the inability of current surveys to detect fossils at these larger distances. In Figure 7, we next use the surface brightness limits from Koposov et al. (2008) to remove any simulated fossil satellite not detectable by current surveys. Using the Koposov et al straight surface brightness cut all but eliminates the fossil population for  $v_{filt} = 20$  km s<sup>-1</sup>. This is a much stronger effect on the detectability of our true fossils than that seen for the Walsh et al. luminosity and distance cuts.

In all distance bins, there is an overabundance of the bright satellites at luminosities typical of the classical dwarfs ( $L_V > 10^5 L_\odot$ ). These should be easily detectable by the SDSS according to Walsh et al. (2009) (assuming the undetected dwarfs have the same distribution of half light radii as the ultra-faints). In Figure 5, the detectable dwarfs are to the right of the dashed line. During our discussion of the missing bright satellites, we use cumulative luminosity functions which have not been corrected for the SDSS limits. We now look at each distance bin individually.

#### 4.2.1. Inner Ultra-Faint Dwarfs at $R < 50$ kpc

In Paper I, we argue that, while the inner ultra-faints have likely lost significant fractions of their stellar populations to tidal stripping, they were not necessarily dIrr at the start of their encounters with the Milky Way. Instead, they may have been more massive primordial fossils. We base this conjecture on Figure 12 in

Paper I which shows that the inner ultra-faints have metallicities,  $[\text{Fe}/\text{H}]$ , that are similar to fossils that are slightly more luminous. But are there enough massive fossils to account for the inner ultra-faints? Figure 8 shows the mass function (bottom) and luminosity function (top) of the pre-reionization halos which are not part of a bound halo at  $z = 0$  and are between 20 kpc and 50 kpc from MW.3. The dotted horizontal lines show the approximate number of stripped fossils required to reproduce the inner ultra-faints. We see that to produce the  $\sim 30$  inner ultra-faints around the Milky Way, we would only need to consider the largest primordial fossils with masses at reionization  $M > 10^8 M_\odot$  and initial luminosities  $L_V > 10^6 L_\odot$ .

#### 4.2.2. $50 \text{ kpc} < R < 100 \text{ kpc}$

A strong piece of evidence for the primordial model would be the total number of observed satellites in one or more radial bins being greater than the number of non-fossils. When we look at  $R < 100 \text{ kpc}$  without the  $R < 50 \text{ kpc}$  cut, we see such an overabundance of observed dwarfs. However, when we do not include the dwarfs within 50 kpc of the galactic center the case is no longer clear cut. If the satellite count from 50 – 100 kpc increases to greater than 25, there is a case for fossils even using the most conservative  $v_{filt} = 20 \text{ km s}^{-1}$ . For  $v_{filt} = 30 \text{ km s}^{-1}$  the number of non-fossils available from 50 – 100 kpc drops to  $\sim 18$ .

For luminosities at which the observational sample is complete, to the right of the dashed lines, we see too many bright ( $L_V > 10^4 L_\odot$ ) objects, even in this inner most radial bin. In addition, as our simulations do not account for post-reionization star formation, it is likely that the overabundance of bright objects is worse than shown in Figure 5. Unless all of the non-fossils have accreted no gas and formed no additional stars after reionization, the simulated curve must lie *below* the observations. This allows these star forming halos to increase in luminosity, shifting the luminosity function of the non-fossils to the right.

#### 4.2.3. $100 \text{ kpc} < R < 200 \text{ kpc}$

In this bin, we probe the outer reaches of the Milky Way’s virial halo and there are a few notable characteristics of the luminosity functions. First, with the addition of the observed dwarfs in this bin, the total number of known satellites around the Milky Way increases to  $\sim 65$ ,  $\sim 45$  not including the inner ultra-faints. The sample at these larger radii is only complete for  $L_V > 10^4 L_\odot$ . For 100 – 200 kpc, with a  $v_{filt} = 20 \text{ km s}^{-1}$  and the less conservative  $v_{filt} = 30 \text{ km s}^{-1}$  there are  $\sim 60$  and  $\sim 40$  simulated non-fossils respectively. Second, the presence of undetected dwarfs is corroborated by the shape of the observed luminosity function around  $10^4 L_\odot$ . Not only is it rising steeply to the detection limit at  $R = 100 \text{ kpc}$ , but its shape is similar to the simulated primordial luminosity function for the true fossils.

In the outer virial halo, we once again overproduce the number of bright satellites. At these radii the discrepancy between theory and observation is more severe than for  $50 \text{ kpc} < R < 100 \text{ kpc}$  since for these radii there is only one observed satellite with  $L_V > 3 \times 10^4 L_\odot$ .

#### 4.2.4. $R > 200$ kpc

For  $R > 200$  kpc, we can only make observational comparisons for  $L_V > 10^5 L_\odot$ . Beyond the virial radius the discrepancy between the observed number of satellites and our simulations is up to  $\sim 1.5$  orders of magnitude, compared with factors of  $\sim 2$  and  $\sim 10$  for the  $50 \text{ kpc} < R < 100 \text{ kpc}$  and  $100 \text{ kpc} < R < 200 \text{ kpc}$  bins, respectively.

### 5. Where are the Bright Satellites?

Our simulations of the fossils of the first galaxies are consistent with the observed Milky Way satellite galactocentric radial distributions (Section 4.1), primordial cumulative luminosity functions (Figure 6), and internal stellar properties (see Paper I). More intriguing, is that at first glance the model appears to fail in the outer parts of the Milky Way by over-producing the number of bright non-fossil satellites. In this section, we explore possible solutions to the bright satellite problem and whether the proposed solutions maintain the agreement between the observed ultra-faint dwarf population and our simulated true fossils. First, we will explore whether the model overestimates the star formation efficiency in pre-reionization dwarfs, and, then, whether we have too many luminous galaxies forming before reionization. It would be of great interest if we could use current observations to constrain galaxy formation models before reionization. We conclude the analysis with a proposal in which the bright satellites do exist in the outer parts of the Milky Way halo but may still be elusive to detection due to their extremely low surface brightnesses. The discovery of these “ghost halos” around known isolated dwarfs is a test of the primordial model and would allow us to determine the efficiency of star formation in the first galaxies.

#### 5.1. Increasing Mass to Light Ratios

First, we explore whether our pre-reionization simulations overestimate the luminosity of galaxies independently of dark matter halo masses. This could be due to using an incorrect IMF in the pre-reionization simulations. We use a mass-to-light ratio for the aged stellar population,

$$\frac{M_*^{rei}}{L} = \left( \frac{M_*^{today}}{L} \right) \left( \frac{M_*^{rei}}{M_*^{today}} \right) \quad (1)$$

where  $M_*^{rei}$  is the mass of the stellar population at reionization, and  $M_*^{today}$  is the mass of the stellar population at  $z = 0$ . The ratio of  $M_*^{rei}/M_*^{today}$  depends on the primordial IMF. The ratio of  $M_*^{rei}/M_*^{today}$  depends on the primordial IMF, and  $M_*^{today}/L \sim 1 - 2$  as for the oldest globular clusters in the Milky Way. A more top heavy IMF for the primordial stars will result in greater stellar mass loss after reionization and fewer low mass stars which can survive to the modern epoch. Conversely, the ratio drops as the primordial IMF produces fewer high mass stars.

To approximate this effect, in Figure 9, we plot the cumulative luminosity functions as in Figure 5, but

increase the stellar mass to light ratio by a factor of 10 in our pre-reionization dwarfs, to  $50M_{\odot}/L_{\odot}$ . The figure shows that increasing the mass to light ratio to  $50M_{\odot}/L_{\odot}$  does not decrease the number of luminous satellites enough to match observations. In the  $50 \text{ kpc} < R < 100 \text{ kpc}$  bin, we can match observations. However, since the primordial luminosities of the non-fossils are only lower limits, the agreement disappears if the population formed *any* stars after reionization. If they did, we are still over-producing luminous satellites. We need to use a mass to light of  $500M_{\odot}/L_{\odot}$  to not over-produce the number of non-fossil satellites in any radial bin. However, this high mass to light ratio makes the fossils virtually dark, with  $L_V < 10^2 L_{\odot}$ .

A blanket suppression of star formation in all halos does not solve the bright satellite problem unless we suppress all star formation in most halos before reionization. We next explore suppression mechanisms which are dependent on the environment or properties of the halos.

## 5.2. Suppression of Pre-Reionization Dwarf Formation in Voids

The formation of  $H_2$  in the early universe is catalyzed by ionizing UV radiation emitted by nearby star forming regions (Ricotti et al. 2002b). In the voids, two factors work against  $H_2$  formation. The delay of structure formation in the voids relative to higher density regions will prevent the minihalos from collapsing until lower redshifts when the  $H_2$  dissociating background is stronger. In addition, the importance of positive feedback is reduced due to the larger mean distances between minihalos in the voids and sources of ionizing radiation (Ricotti et al. 2002a,b, 2008). The combination of these factors may result in a reduced abundance of  $H_2$  relative to the regions around a Milky Way. This may produce a star formation efficiency before reionization that depends on the environment. We approximate the most extreme case of  $H_2$  suppression in the voids by suppressing all star formation in halos in regions with  $\delta \lesssim 0.4$ . The extreme suppression of the star formation in the voids we use treats all halos but those in the overdense regions ( $z_{eff} = 8.3$ ) as dark.

Since the bright satellite problem is most prominent in the outer regions of the Milky Way halo, the lack of star formation in low density regions may decrease the number of bright halos beyond the virial radius while leaving the satellite luminosity functions unchanged at smaller radii and lower luminosities. However, Figure 11 shows that, even in the most extreme case, suppressing  $H_2$  formation in the voids does not decrease the number of bright satellites enough in any radial bin to bring our simulations into agreement with observations. In this scenario, there is no appreciable reduction of the number of bright satellites for  $R < 200 \text{ kpc}$ . There is a decrease in the luminosity function at larger radii, but it is neither strong or focused enough on the high luminosity subhalos to solve the overabundance of bright satellites in the outer parts of the Milky Way. Enough of the region within 1 Mpc of our Milky Way is at the highest density in our simulation ( $z_{eff} = 8.3$ ) that the complete suppression of star formation in even moderately less dense regions does not sufficiently change the luminosity functions or radial distributions.

With the inability of  $H_2$  suppression in the voids and overall suppression of star formation to account for the missing bright satellites, we shift our focus to properties of the halos which vary with halo mass.

### 5.3. Lowering the Star Forming Efficiency

In the pre-reionization simulations, the sub-grid recipe for star formation depends on a free parameter,  $\epsilon_*$ , controlling the efficiency of conversion of gas into stars per unit dynamical time. One of the main results of the pre-reionization simulations is that the global star formation rate and  $f_*(M) = M_*/M_{bar}$  (the fraction of total mass converted into stars, where  $M_{bar} = M/7.5$ ) is nearly independent of  $\epsilon_*$  in small mass dwarfs due to the self-regulation mechanisms of star formation. However, in halos with masses  $M \gtrsim 5 - 10 \times 10^7 M_\odot$ ,  $f_*(M)$  is typically proportional to  $\epsilon_*$  since the higher mass minihalos are less sensitive to self-regulation feedback. We used  $\epsilon_* = 5\%$  in our fiducial runs, that may be too large (*e.g.*, Trenti et al. 2010). The pre-reionization simulations may have overestimated the luminosity of primordial dwarfs with  $M \gtrsim 5 \times 10^7 M_\odot$ , for which the  $f_*$  vs  $M$  relationship is tighter. We explore the effect of reducing  $\epsilon_*$  by introducing a maximum stellar fraction,  $f_{*,crit}$ . Roughly,  $f_{*,crit}$  corresponds to the mass threshold where feedback effects no longer dominate and where the value of  $\epsilon_*$  becomes important. If we reduce  $f_{*,crit}$ , we will decrease the luminosities of our most luminous halos. Roughly, for halo masses  $M \sim 3 \times 10^7 M_\odot$  (virial mass at formation) our simulations have  $f_*(M) \sim 1\%$ . This is in agreement with observed values for dwarfs with  $v_c \sim 10 \text{ km s}^{-1}$  (McGaugh et al. 2010).

Figure 12 shows the luminosity functions of our simulations with all halos with  $f_{*,crit} = 1\%$  (left panel) and  $f_{*,crit} = 0.1\%$  (right panel). The figure shows that lowering the star formation efficiency preferentially for the higher mass halos is effective in decreasing the number of non-fossil subhalos with  $L_V > 10^5 L_\odot$ . Adopting  $f_{*,crit} = 1\%$  decreases the number of luminous halos enough to bring the luminosity functions in agreement with observations, while preserving the agreement for the fossil population. However, in the radial bins  $50 \text{ kpc} < R < 500 \text{ kpc}$ , there still are too many subhalos with  $L_V > 10^5 L_\odot$ , though the discrepancy has dropped significantly. Coupling a lower  $\epsilon_*$  with a higher mass to light ratio or  $H_2$  suppression in the voids does not correct the remaining bright satellite overabundance. However, when we set  $f_{*,crit} = 0.1\%$ , the cumulative primordial luminosity function of our simulated dwarfs becomes consistent with observations at all radii, but requires a deduction of  $f_*$  in halos with mass  $M \sim 7 \times 10^6 M_\odot$  whose  $f_*$  is self-regulated and thus independent of  $\epsilon_*$  (Ricotti et al. 2002b).

Any solution for the overabundance of bright satellites must preserve not only the existence of the true fossil population, but also its distribution and properties. We next look at the other dimensions of the agreement between the true fossil populations with an  $f_{crit} = 1\%$  and  $0.1\%$  and the ultra-faints and classical dSph. Figure 13 shows the radial distribution of the true fossils around MW.2 and MW.3 from Run D the observed Milky Way population for an  $f_{crit} = 1\%$ . While for  $10^3 L_\odot < L_V < 10^4 L_\odot$  and  $10^4 L_\odot < L_V < 10^5 L_\odot$  the fossil population with  $f_{crit} = 1\%$  reproduces the observed radial distribution, we no longer have any true fossils with  $L_V > 10^5 L_\odot$ . If the star formation efficiency of our pre-reionization halos is lowered enough to bring the number of luminous satellites in line with observations, the fossil luminosity threshold discussed in Paper I is dropped to  $L_V < 10^5 L_\odot$ . For  $f_{crit} = 0.1\%$  the threshold drops further to  $10^4 L_\odot$ .

The loss of the multi-dimensional agreement between our true fossils and the ultra-faints shows that lowering  $\epsilon_*$  enough to account for the missing luminous satellites is not a viable solution for the bright



satellite problem if the ultra-faint dwarfs are fossils of the first galaxies. In this interpretation, we need a different mechanism which will either preferentially suppress star formation in the most luminous pre-reionization halos to a greater degree, or cause their lower redshift counterparts to lose the majority of their primordial stellar population after reionization. If neither of these solutions work, we must ask ourselves if the halos CDM predicts are there at all.

#### 5.4. The Ghost Halos

As discussed in Paper I, our N-body method does not allow us to determine the dynamics of the stars in halos that undergo mergers, or the degree to which those stars are tidally stripped. However, we have used analytic relationships to estimate the importance of dynamical heating of the stars when  $z = 0$  fossils (about 20%) are produced by mergers of more than one pre-reionization dwarf (Paper I) We refer to such interactions as galaxy mergers. Here, we focus on those dynamical processes in non-fossils which result in the dispersion of the primordial stellar populations of the brightest satellites, the net effect of which is to either make the non-fossil populations invisible to current surveys by reducing their surface brightnesses below the SDSS detection limits or preferentially stripping them during interactions with more massive halos. The former mechanism would be relevant to non-fossils at  $R \gtrsim 500$  kpc where tidal forces are negligible.

The number of pre-reionization halos in a  $z = 0$  dwarf increases with mass. In this section, we explore the role of mergers to rend invisible, or strip, the primordial populations of stars in the the more massive dwarfs (non-fossils). Unlike in the previous sections, here we differentiate between the non-fossils and polluted fossils in our simulations. We remind the reader, that though both populations have  $v_{max}$  which were large enough for them to accrete gas from the IGM in the past, only the non-fossils are at or above that threshold at  $z = 0$ .

When a system undergoes a galaxy merger, kinetic energy from the collision is imparted to the stars. Immediately after the collision, the new system will be in its most diffuse state. We define a galaxy merger as the interaction of two or more pre-reionization halos, both containing a primordial stellar population. Although there is significant scatter in the luminosities of minihalos of the same mass, in general, the luminous minihalos are more massive than those which are dark. An interaction between two luminous minihalos is therefore more significant. We use  $N_{lum}$ , the number of luminous pre-reionization halos within at  $z = 0$  halo, as a proxy for the number of galaxy mergers. If there are multiple galaxy mergers in a short amount of time, these stars will be susceptible to stripping. In addition, recent work on increasing the extent of the stellar population in bright ellipticals from  $z = 2$  to  $z = 0$  suggests that many minor interactions over several Gyrs can increase the size of the galaxy by a factor of 2-5 without significantly increasing mass (Naab et al. 2009). Roughly, the larger the number of significant interactions, the greater the spatial extent of the pre-reionization population and more likely the halo will have lost a significant fraction of its primordial population to dynamical heating.

For isolated halos, with large  $N_{lum}$ , the radius of the primordial population increases, possibly until

it fills the spatial extent of the dark matter halo. Such an extended system would have extremely low surface brightness and would be susceptible to tidal stripping. We next look at which of our three subhalo populations has a significant number of members with  $N_{lum} > 3$ . The fractions of the true fossil, and non-fossils populations with a given  $N_{lum}$  are shown in the left and right panels of Figure 14. Neither of the fossil populations has a significant fraction of subhalos with  $N_{lum} > 3$  with the fractions at  $\sim 1\%$  and  $\sim 10\%$  respectively. We therefore assume, that, while a few of our true and polluted fossils may have had their primordial populations diffused by mergers, the vast majority remain dynamically cold.

The non-fossils show the opposite trend. The right panel of Figure 14 shows that  $< 10\%$  of the non-fossils have  $N_{lum} < 3$  and the distribution peaks at  $N_{lum} \sim 5$ . A population of non-fossils would be much more likely to have a primordial population dispersed by multiple major interactions than their fossil counterparts.

The non-fossil populations (see Figure 5) could have either lost their stellar populations, or had their primordial populations increase in size to the point where they are undetectable by the SDSS. Near the Milky Way, we assume they lost their entire primordial stellar population to tidal interactions. After falling into the Milky Way halo, the non-fossils were unable to form a significant younger stellar population.

At larger radii, the non-fossils are less likely to have their primordial populations stripped. However, as the stars expand to fill the spatial extent of the dark matter halo, the non-fossils end up with a primordial population with  $\Sigma_V \sim L_V \times R_p^{-2}$ , where  $L_V$  is the luminosity of the primordial population and  $R_p$  is the radius of the primordial population. Figure 15 shows the fraction of the non-fossils with a primordial population with surface brightness,  $\Sigma_V$ , for  $R_p = R_{max}$  and  $R_p = 0.25 \times R_{max}$ , where  $R_{max}$  is the radius of the maximum circular velocity. We find that for  $R_p = R_{max}$  about 1% of non-fossils would have an extended primordial halo above the SDSS detection limits (to the right of the dashed line), and, when  $R_p$  is decreased to  $0.25 \times R_{max}$ , the detectable fraction only rises to 20%. If these non-fossils formed few or no stars after reionization the majority would be undetectable by SDSS. The non-fossils which did form stars after reionization today could be dIrr or one of the few isolated dSphs or dSphs/Irrs: *e.g.*, Cetus, Tucana, Antlia. In our scenario, they would be surrounded by “ghost halos” of primordial stars  $\sim 12$  Gyr old with  $[Fe/H] \lesssim -2$ . But does the dispersal of the primordial population into “ghost halos” solve the “bright satellite problem”?

We quantitatively approximate this for our simulations by using a circular velocity cut. We look at the primordial luminosity functions as if all the ghost halos are either stripped or below SDSS detection limits. Practically, we set the luminosities to zero for all the non-fossils. We look to see if this cut solves the bright satellite problem while preserving the fossils better than lowering the star formation efficiency. We find it to be a good solution to the bright satellite problem.

Since setting the non-fossils luminosities to zero is able to decrease the number of luminous satellites, we look at the luminosity function it produces in more detail. All the curves in Figure 16 are the same as in Figure 5, excepting the red curve for the non-fossils that now represents only the polluted fossils.

We now look at each distance bin to see what turning off the non-fossil population has done to our various arguments. For  $50 \text{ kpc} < R < 100 \text{ kpc}$ , the necessity of a primordial dwarf population is even

stronger when we only consider the fossil and polluted fossil populations. There are only  $\sim 7$  polluted fossils within 100 kpc, less than one-fifth of what is required to account for the  $\sim 50$  observed satellites. For  $L_V > 10^4 L_\odot$ , the luminosity function now sits below observations. This gives the remaining star forming halos room to form additional stars without overproducing subhalos with  $L_V > 10^4 L_\odot$ . The total number of subhalos within 100 kpc decreasing to 35 is consistent with observations. First, our MW.3 is on the low end of the mass range for the Milky Way for both observational estimates and simulations. Second, as seen in Figure 8, there are more than enough stripped down fossils which formed in halos with  $M > 10^7 M_\odot$  and  $L_V > 10^5 L_\odot$  to fill in the deficit. Since these objects would lack a cloud of tracer particles, they are marked as unbound by the halo finder AHF and would be included in the luminosity and mass of the host halo and not in any luminosity function of the satellites.

The complete invisibility of the non-fossils is not quite as successful for  $100 \text{ kpc} < R < 200 \text{ kpc}$  as we are still slightly overproducing the number of  $L_V > 10^5 L_\odot$  satellites compared to observations. However, we are better able to reproduce the sudden steepening in the observed luminosity function in Figure 16 than with any of our other suppression mechanisms (Figures 10, 11, and especially 12). This feature may be unique to the Milky Way so we are not unduly concerned with matching it. In addition, if the non-fossils are dark, our argument for the existence of primordial fossils becomes straightforward. There are only  $\sim 30$  polluted fossils in this distance bin, only 75% of the  $\sim 40$  observed galaxies, with any dwarf with  $L_V < 10^4 L_\odot$  difficult, if not impossible, to detect with current surveys.

Beyond the MW.3 virial radius ( $R \sim 200 \text{ kpc}$ ), turning the non-fossils dark easily places the primordial luminosity function into agreement with observations. This allows for the formation of post-reionization populations of stars in the polluted fossils and non-fossils. We remind the reader that the  $z = 0$  halos at these radii would likely be on first approach to the Milky Way system and more likely to accrete and retain gas at later times. The diffuse primordial population in these distant non-fossils is an observational test of star formation in pre-reionization dwarfs and the existence of pre-reionization fossils.

## 6. Three Observational Tests and Model Predictions

Although the existence of pre-reionization fossils seems likely, observations do not unequivocally demonstrate their existence due to the large uncertainties in estimating the number of yet undiscovered ultra-faint dwarfs (Tollerud et al. 2008). In this section, we summarize three observational tests for the existence of fossils of the first galaxies that we propose based on the results in Paper I and the present work. The first test of our model is especially interesting as it can be performed using HST observations and does not require waiting for future all sky surveys deeper than SDSS, like PanStar or LSST, to be online.

### 1. “Ghost halos” around dwarfs on the outskirts of the Local Group

The primordial stellar populations in minihalos that formed before reionization should produce diffuse “ghost halos” of primordial stars around isolated dwarfs. We have shown that the total luminosity of the “ghost halos” is comparable to the one of classical dwarfs, but the surface brightness of the stars

is well below the SDSS detection limits. Contrary to the difficulties of finding ultra-faints, we know where these diffuse stars are and we can plan deep observations to detect them. The diffuse primordial stellar populations around non-fossils should not be tidally stripped in dwarfs with galactocentric distance  $> 1$  Mpc from the Milky Way. We do not know within which distance tidal stripping would become important, but due to their large half light radii, they certainly are the stellar population that would be stripped first. “Ghost halos” can be best detected by resolving their individual main sequence stars around isolated dIrrs or dSphs before using spectra to determine their metallicities and dynamics. Unlike younger stars dispersed from the central galaxy, the primordial ghost halo would have a  $[Fe/H] < -2.5$ , and we are currently running simulations to determine their dynamics.

Recent HST observations of M31 have resolved the main sequence using ACS (Brown et al. 2006, 2008, 2009). A low-luminosity dwarf at  $\sim 800$  kpc on the other side of the Milky Way from M31 would be an excellent candidate for the ghost halo search, and detection of its main-sequence primordial stars would be within the reach of HST. At 800 kpc, the field of view of WFC3 (162”) is  $\sim 630$  pc, at 1 Mpc,  $\sim 785$  pc, and at 2 Mpc,  $\sim 1.6$  kpc. The ghost halos are  $> 1$  kpc in radius, often up to a few tens of kpc, therefore, WFC3 would not be able to image the entire dwarf with its ghost halo. However, aimed at the outskirts of a likely ghost halo host, it could look for signs of a primordial halo in the color magnitude diagram and radial surface brightness distribution. We would be able to resolve the individual stars in the ghost halos at  $\sim 1$  Mpc. The ghost halos have surface densities of stars of 0.001 and 1 star  $\text{pc}^{-2}$  depending on the extent of the ghost halos and the slope of the IMF at low masses. Assuming a stellar density of 1 star  $\text{pc}^{-2}$ , the angular distance between each star is  $\sim 0.26''$ , larger than the WFC3 resolution of  $0.04''$  per pixel. Since the stellar population can be resolved, determining the details of a ghost halo population is a matter of taking deep enough exposure to detect the main sequence stars. Red giant branch stars, while brighter and easier to detect, have a density three orders of magnitude lower than the main sequence.

Deep observations work well for detecting the ghost halos when we already know where they are. These primordial populations surround dwarf galaxies that have undergone significant star formation since reionization and may have detectable gas and active star formation today. However, as discussed in § 5.4, in order to reproduce the observed satellite distribution, only a fraction of the ghost halos can have formed a significant younger stellar populations. We remind the reader that our definition of a fossil versus a non-fossil in the simulations assumes a constant  $v_{filter} = 20 \text{ km s}^{-1}$ . Assuming a larger filtering velocity produces a smaller number of non-fossils, some of the halos we define as non-fossils, and containing ghost halos, may have been unable to accrete gas and form stars after reionization due to additional heating of the IGM. This population of “dead” ghost halos would have only an extremely diffuse, primordial population. Without H I or more concentrated, younger stars, the best chance for detecting these ghost halos would be large scale surveys. Figure 15 shows that the majority of the ghost halos are beyond the reach of the SDSS, but what about upcoming, deeper surveys such as PanSTARRS?

Diffuse stellar systems like the ultra-faint dwarfs and the ghost halos are found in surveys by looking for overdensities of stars relative to the background. In many cases, by detecting stars at the tip of the red giant branch (RGB). In low luminosity systems the detection of the RGB depends on two factors,

the distance to the halo and the population of the RGB. Low luminosity systems, like the ultra-faint dwarfs, can have as few as a thousand stars, and therefore a sparsely populated, and difficult to detect, RGB. For example, with SDSS (magnitude limit  $r = 22.5$ ) Hercules ( $1.1 \times 10^4 L_{\odot}$ ) could only be detected to 300 kpc, while the more luminous CVn I ( $2.3 \times 10^5 L_{\odot}$ ) would be seen at a Mpc from the Milky Way (Koposov et al. 2008). PanSTARRS (magnitude limit  $r=24$ ) will reach 1.5 magnitudes deeper than SDSS, detecting the same RGB twice as far. However, the primordial populations in the ghost halos are *extremely* diffuse, and it is unclear that the overdensity of their RGB stars would be high enough to be detected against foreground M dwarfs and distant galaxies. In short, while PanSTARRS is expected to detect new ultra-faint dwarfs, it may not be the best tool for finding ghost halos.

If some of the discovered ultra-faint dwarfs are fossils, then “ghost halos” should exist. Vice versa, the detection of “ghost halos,” regardless of the method, can be used to constrain the star formation rates before reionization and would imply the existence of fossils, although these fossils may not have yet been discovered due to their low surface brightnesses.

## 2. *Population of yet undetected ultra-faint dwarfs*

In BR09 and Paper I we have discussed in detail the existence and the properties of a yet undetected population of fossils with  $L_V < 10^4 L_{\odot}$  and surface brightness  $\Sigma_V < 10^{-1.4} L_{\odot} \text{ pc}^{-2}$ . This population of ultra-faints should be accessible to future all sky surveys such as PanStars and LSST. If the undetected dwarfs are fossils, they should have stellar velocity dispersions equivalent to those of the ultra-faints with corresponding mass to light ratios of  $10^4 M_{\odot}/L_{\odot}$  or higher. The typical  $[Fe/H]$  of the “stealth” fossils should be  $< -2.5$ . We direct the reader to Paper I for a detailed justification of these predictions.

## 3. *Dark and ultra-faint gas rich dwarfs in the voids*

According to the model proposed in Ricotti (2009), a subset of minihalos in the voids may have been able to condense gas from the IGM after Helium II reionization (at  $z \sim 3$ ). However, they would not form stars unless their gas reached a sufficient density. These minihalos may or may not have formed stars before reionization, and any stellar populations they did have would be below the detection limits of both current and future surveys. The HI in these objects could be detected by blind 21 cm surveys. Recently, ALFALFA and GALFA surveys have reported the discovery of several small and compact clouds of neutral hydrogen, some of which may represent a population of pre-reionization minihalos. Some of these clouds could be “dark galaxies” and represent the smallest detectable halos around the Milky Way, others may be ultra-faint dwarfs in the voids. The location of unassociated HI detections could then guide optical surveys to these primordial fossils in a focused deep search for their ancient populations.

## 7. Summary and Discussion

Through this work and Paper I, we have used results of simulations to study the origin of observed Milky Way and M31 satellites and understand whether they are compatible with models of star formation before reionization. In the primordial model, a subset of the Milky Way satellites formed with their current properties with minimal modifications by tidal stripping. These low luminosity satellites formed the majority ( $> 70\%$ ) of their stars in minihalos before reionization. Our simulated true fossils produce an excellent agreement in properties and distribution with the observed lowest luminosity Milky Way satellites. In BR09 and Paper I, we showed that a subset of the ultra-faints, all with  $L_V < 10^5 L_\odot$ , have half-light radii, surface brightnesses, mass-to-light ratios, velocity dispersions, metallicities and metallicity dispersions consistent with the expected stellar properties of the true fossils. In the present paper, we have compared the galactocentric radial distributions and primordial cumulative luminosity functions of simulated fossils to observations of Milky Way satellites. When we compare the observed and simulated distributions, we find them to be in agreement with each other for  $L_V < 10^5 L_\odot$ . In addition, a large population of primordial fossils have surface brightness below the detection limits of current surveys (*e.g.*, SDSS). The following list summarizes the main results of this second paper of the series.

- We are able to reproduce the distribution of the ultra-faints with our simulated primordial fossils. We find no missing satellites at the lower end of the mass and luminosity functions, but our model predicts  $\sim 150$  additional Milky Way satellites detectable by upcoming surveys (PanStars, LSST). In addition to the undiscovered “missing” satellites at distances too great ( $\gtrsim 50$ -100 kpc) to be detected by SDSS or in areas on the sky not in the SDSS footprint, there is also a new population of ultra-faints with mega-faint surface brightness hidden below the SDSS detection limits at all distances from the Milky Way.
- At all radii, we find an overabundance of simulated bright ( $L_V > 10^4 L_\odot$ ) satellites with respect to observations, which, even with only their primordial luminosities, would be easily detected by current surveys if we assume they have the same half-light radii as the other known ultra-faint dwarfs. Given the agreement between the stellar properties and distributions of the ultra-faints and those of our fossil dwarfs, we cannot account for the excess bright satellites by imposing a blanket suppression of star formation below a given mass.
- Lower  $H_2$  formation rates and subsequent lower minihalo star formation rates in the voids are not able to bring the number of bright satellites into agreement with observations.
- Effectively lowering the star formation efficiency can fix the bright satellite problem if we assume only pre-reionization halos with  $M < 7 \times 10^6 M_\odot$  had SFR dominated by local, stochastic feedback. However, not only is this contrary to current understanding of star formation in minihalos, but the fossil population this “solution” produces cannot reproduce the distribution of the ultra-faint population.
- We bring the number of bright satellites into agreement with observations, while leaving the fossil population untouched, by assuming the primordial stellar populations of our non-fossils (with max-

imum circular velocities,  $v_{max}(z = 0) > v_{filt}$ ) become extremely diffuse via kinetic energy from galaxy mergers. The existence of “ghost halos” of primordial stars is a new powerful observational prediction of our model that can be straight forwardly tested using HST observations of isolated dwarfs around the Local Group.

One of the key predictions of the primordial model is a total number of satellites for the Milky Way between 200 – 300, only a maximum of 100 of which are non-fossils (here we assumed  $v_{filt} = 20 \text{ km s}^{-1}$ ). The number of Milky Way satellites which are not fossils provides an important test for star formation in minihalos at high redshift. If, after PanSTARRS and LSST are online, the number of ultra-faint Milky Way satellites remains  $< 100$ , we have a strong constraint on star formation in pre-reionization dwarfs. Either no pre-reionization fossils survived near the Milky Way, or almost none of the halos with masses at formation  $M < 10^8 M_{\odot}$  formed stars. However, if the satellite count rises to  $> 100$ , some of the dimmest Milky Way dwarfs must be fossils of reionization. Using details of the stellar populations and their distributions, observations of these fossils can constrain models of star formation at high redshift.

A caveat to this picture is that the number of non-fossils is highly sensitive to the choice of the filtering velocity. When we raise the filtering velocity to  $30 \text{ km s}^{-1}$ , the number of non-fossils drops by a third to  $60 \pm 8$  from the  $90 \pm 10$  for  $v_{filt} = 20 \text{ km s}^{-1}$ . The choice of  $20 \text{ km s}^{-1}$  assumes a constant IGM density with  $T_{IGM} = 10^4 \text{ K}$  throughout a minihalo’s evolution. In reality, the situation is not so simple. The gas near  $10^{12} M_{\odot}$  halos and in the filaments between may be heated to  $\sim 10^5 - 10^6 \text{ K}$  by AGN feedback. The higher temperatures of this local intergalactic medium may correspond to  $v_{filt} \gtrsim 40 \text{ km s}^{-1}$ . In addition to the higher filtering velocity, the higher density near a Milky Way mass halo reduces the effective potential depth of the subhalos, increasing the mass threshold for post-reionization gas accretion still further. Simulations to determine the temperature and density of the IGM near a Milky Way from reionization to the modern epoch are needed to determine the  $v_{filt}(\mathbf{x}, z)$ , and whether these factors can explain the existence of Milky Way and M31 dwarfs with the observed properties of fossils, but luminosities above the  $10^6 L_{\odot}$  threshold.

The observed distributions we compare to depend on how we correct for the incomplete sky coverage of the SDSS. In this work, we have assumed an isotropic satellite distribution at  $R > 50 \text{ kpc}$ . Under this assumption, the SDSS completeness correction for the ultra-faints is 3.54. We briefly check if the agreement between the observed and simulated distributions is dependent on the isotropic assumption. Recent work (Metz et al. 2007, 2009) has suggested that rather than being isotropic, the Milky Way satellites are oriented in a plane approximately perpendicular to the disk. We approximate this non-homogeneous satellite distribution by correcting for the SDSS sky coverage by a factor of 2.0 instead of 3.54. The number of classical fossils remains the same. The different correction does not change the consistency of our simulated galactocentric distribution with observations, though the lower correction factor suggests a higher Milky Way mass. It also does not change the bright satellite problem, in fact, the lower observational correction factor makes the overabundance of simulated  $L_V > 10^4 L_{\odot}$  dwarfs worse by about a factor of two.

We have suggested two solutions which correct for the overabundance of bright satellites while preserving at least a fraction of the primordial fossil population. Each presents a different picture when we consider it in the context of the voids. The first, and less effective, solution calls for a low star formation

efficiency. In this picture, the  $10^{10} M_{\odot}$  halos visible in current surveys will have their star formation dampened, however as we move to  $10^7 M_{\odot}$  we enter the regime where stochastic feedback effects dominate over the choice of  $\epsilon_*$ . Thus, the voids would appear relatively empty, but only because we cannot yet detect the less than  $10^5 L_{\odot}$  fossil populations which formed in the  $10^7 M_{\odot}$  halos before reionization.

The dispersal of the non-fossils’ primordial populations into ghost halos is a more effective solution to the “bright satellite problem” within 1 Mpc of the Milky Way, but leaves a conundrum in the voids. Regardless of whether the primordial population would be detectable, how do we keep the post-reionization star formation in these non-fossils low enough to prevent this later star formation from producing more  $M_V > -16$  galaxies than are currently observed?

Any post-reionization star formation in the non-fossils results in a young population which would be (i) brighter and bluer, (ii) more concentrated, since enriched gas will cool faster and sink deeper into the gravitational potential, and (iii) possibly accompanied by an H I reservoir. Any of these properties would make the post-reionization population easier to see, and the non-fossil harder to hide. To suppress the post-reionization baryonic evolution in the non-fossils we examine our naive assumption that they all undergo significant baryonic evolution after reionization.

The easiest way to suppress star formation in the lower mass non-fossils is to raise the filtering velocity. As has already been discussed in Chapter 4, any non-fossil embedded in the WHIM ( $T \sim 10^5$  K) would have a  $v_{filter} \sim 40 \text{ km s}^{-1}$ . However, the WHIM does not exist until  $z < 1$  (Smith et al. 2010), leaving  $\sim 6$  Gyr after reionization when the non-fossils could have accreted gas and formed stars. Active galactic nuclei (AGN) eject enormous amounts of energy into their environs, heating the gas and raising the filtering velocity, but how far from the host galaxy the AGN is effective at suppressing star formation in dwarfs, and for how long is unclear. In addition, we see a bright satellite problem around every large Local Volume galaxy. Is it reasonable to assume that, at some point in its evolution, every  $L_*$  galaxy hosted an AGN? A final possibility is that reionization was extremely efficient at quenching star formation in  $20 - 40 \text{ km s}^{-1}$  halos and the non-fossils were never able to build up enough gas from the post-reionization IGM to form additional stars.

In summary, while the bright satellite problem can be “solved” for the primordial population alone, we still need to account for the post-reionization evolution of the non-fossils. In order to maintain the agreement with observations, only  $\sim 10\%$  of the non-fossils can form significant stellar populations after reionization. Determining how and if the other  $\sim 90\%$  can be suppressed will tell us how much of a problem the bright satellite problem is.

The simulations presented in this paper were carried out using computing clusters administered by the Center for Theory and Computation of the Department of Astronomy at the University of Maryland (“yorp”), and the Office of Information Technology at the University of Maryland (“hpcc”). This research was supported by NASA grants NNX07AH10G and NNX10AH10G. The authors thank the anonymous referee for constructive comments and feedback. Thanks from MSB and MR to Stacy McGaugh, Derek Richardson and Rosie Wyse for helpful conversations and comments. MSB would like to thank Susan



Lamb for discussions of dwarf dynamics and Evan Kirby and Beth Willman for discussions of modeling and observations.

## REFERENCES

- Abazajian, K. N., et al. 2009, *ApJS*, 182, 543
- Ahn, K., Shapiro, P. R., Alvarez, M. A., Iliev, I. T., Martel, H., & Ryu, D. 2006, *New Astronomy Review*, 50, 179
- Bailin, J., Power, C., Norberg, P., Zaritsky, D., & Gibson, B. K. 2008, *MNRAS*, 390, 1133
- Barkana, R., & Loeb, A. 2004, *ApJ*, 609, 474
- Belokurov, V., et al. 2007, *ApJ*, 654, 897
- Belokurov, V., et al. 2006, *ApJ*, 647, L111
- Bovill, M. S., & Ricotti, M. 2009, *ApJ*, 693, 1859
- Bozek, B., Wyse, R. F. G., & Gilmore, G. F. 2011, in *Bulletin of the American Astronomical Society*, Vol. 43, American Astronomical Society Meeting Abstracts #217, 147.06
- Brown, T. M., et al. 2008, *ApJ*, 685, L121
- Brown, T. M., et al. 2009, *ApJS*, 184, 152
- Brown, T. M., Smith, E., Ferguson, H. C., Rich, R. M., Guhathakurta, P., Renzini, A., Sweigart, A. V., & Kimble, R. A. 2006, *ApJ*, 652, 323
- Bullock, J. S., Kravtsov, A. V., & Weinberg, D. H. 2001, *ApJ*, 548, 33
- Bullock, J. S., Stewart, K. R., Kaplinghat, M., Tollerud, E. J., & Wolf, J. 2010, *ApJ*, 717, 1043
- Ciardi, B., Ferrara, A., & Abel, T. 2000, *ApJ*, 533, 594
- Cioni, M.-R. L., & Habing, H. J. 2005, *A&A*, 442, 165
- de Jong, J. T. A., et al. 2008, *ApJ*, 680, 1112
- Efstathiou, G. 1992, *MNRAS*, 256, 43P
- Frebel, A., Simon, J. D., Geha, M., & Willman, B. 2010, *ApJ*, 708, 560
- Geha, M., Willman, B., Simon, J. D., Strigari, L. E., Kirby, E. N., Law, D. R., & Strader, J. 2009, *ApJ*, 692, 1464
- Haiman, Z., Abel, T., & Rees, M. J. 2000, *ApJ*, 534, 11

- Irwin, M. J., et al. 2007, *ApJ*, 656, L13
- Karachentsev, I. D., et al. 2006, *AJ*, 131, 1361
- Karachentsev, I. D., Karachentseva, V. E., Huchtmeier, W. K., & Makarov, D. I. 2004, *AJ*, 127, 2031
- Klypin, A., Kravtsov, A. V., Valenzuela, O., & Prada, F. 1999, *ApJ*, 522, 82
- Knollmann, S. R., & Knebe, A. 2009, *ApJS*, 182, 608
- Koposov, S., et al. 2008, *ApJ*, 686, 279
- Kravtsov, A. 2010, *Advances in Astronomy*, 2010
- Kroupa, P., Theis, C., & Boily, C. M. 2005, *A&A*, 431, 517
- Macciò, A. V., Kang, X., Fontanot, F., Somerville, R. S., Koposov, S., & Monaco, P. 2010, *MNRAS*, 402, 1995
- Machacek, M. E., Bryan, G. L., Meiksin, A., Anninos, P., Thayer, D., Norman, M., & Zhang, Y. 2000, *ApJ*, 532, 118
- Maio, U., Ciardi, B., Dolag, K., Tornatore, L., & Khochfar, S. 2010, *MNRAS*, 905
- Martinez, G. D., Minor, Q. E., Bullock, J., Kaplinghat, M., Simon, J. D., & Geha, M. 2010, *ArXiv e-prints*
- Mateo, M. L. 1998, *ARA&A*, 36, 435
- McGaugh, S. S., Schombert, J. M., de Blok, W. J. G., & Zagursky, M. J. 2010, *ApJ*, 708, L14
- McGaugh, S. S., & Wolf, J. 2010, *ArXiv e-prints*
- Metz, M., Kroupa, P., & Jerjen, H. 2007, *MNRAS*, 374, 1125
- Metz, M., Kroupa, P., & Jerjen, H. 2009, *MNRAS*, 394, 2223
- Monelli, M., et al. 2010, *ApJ*, 720, 1225
- Moore, B., Ghigna, S., Governato, F., Lake, G., Quinn, T., Stadel, J., & Tozzi, P. 1999, *ApJ*, 524, L19
- Naab, T., Johansson, P. H., & Ostriker, J. P. 2009, *ApJ*, 699, L178
- Niederste-Ostholt, M., Belokurov, V., Evans, N. W., Gilmore, G., Wyse, R. F. G., & Norris, J. E. 2009, *MNRAS*, 398, 1771
- Norris, J. E., Wyse, R. F. G., Gilmore, G., Yong, D., Frebel, A., Wilkinson, M. I., Belokurov, V., & Zucker, D. B. 2010, *ArXiv e-prints*
- O’Shea, B. W., & Norman, M. L. 2008, *ApJ*, 673, 14

- Peebles, P. J. E. 2001, *ApJ*, 557, 495
- Ricotti, M. 2009, *MNRAS*, 392, L45
- Ricotti, M. 2010, *Advances in Astronomy*, 2010
- Ricotti, M., & Gnedin, N. Y. 2005, *ApJ*, 629, 259
- Ricotti, M., Gnedin, N. Y., & Shull, J. M. 2000, *ApJ*, 534, 41
- Ricotti, M., Gnedin, N. Y., & Shull, J. M. 2001, *ApJ*, 560, 580
- Ricotti, M., Gnedin, N. Y., & Shull, J. M. 2002a, *ApJ*, 575, 33
- Ricotti, M., Gnedin, N. Y., & Shull, J. M. 2002b, *ApJ*, 575, 49
- Ricotti, M., Gnedin, N. Y., & Shull, J. M. 2008, *ApJ*, 685, 21
- Ricotti, M., & Ostriker, J. P. 2004, *MNRAS*, 352, 547
- Ricotti, M., Ostriker, J. P., & Gnedin, N. Y. 2005, *MNRAS*, 357, 207
- Sand, D. J., Olszewski, E. W., Willman, B., Zaritsky, D., Seth, A., Harris, J., Piatek, S., & Saha, A. 2009, *ApJ*, 704, 898
- Simon, J. D., & Geha, M. 2007, *ApJ*, 670, 313
- Simon, J. D., et al. 2010, *ArXiv e-prints*
- Smith, B. D., Hallman, E. J., Shull, J. M., & O’Shea, B. W. 2010, *ArXiv e-prints*
- Springel, V. 2005, *MNRAS*, 364, 1105
- Strigari, L. E., Bullock, J. S., Kaplinghat, M., Simon, J. D., Geha, M., Willman, B., & Walker, M. G. 2008, *Nature*, 454, 1096
- Thoul, A. A., & Weinberg, D. H. 1996, *ApJ*, 465, 608
- Tikhonov, A. V., & Klypin, A. 2009, *MNRAS*, 395, 1915
- Tinker, J. L., & Conroy, C. 2009, *ApJ*, 691, 633
- Tollerud, E. J., Bullock, J. S., Strigari, L. E., & Willman, B. 2008, *ApJ*, 688, 277
- Trenti, M., Stiavelli, M., Bouwens, R. J., Oesch, P., Shull, J. M., Illingworth, G. D., Bradley, L. D., & Carollo, C. M. 2010, *ApJ*, 714, L202
- Tully, R., et al. 2006, *ArXiv Astrophysics e-prints*
- Venkatesan, A., Giroux, M. L., & Shull, J. M. 2001, *ApJ*, 563, 1

- Walker, M. G., Mateo, M., Olszewski, E. W., Peñarrubia, J., Wyn Evans, N., & Gilmore, G. 2009, *ApJ*, 704, 1274
- Walker, M. G., McGaugh, S. S., Mateo, M., Olszewski, E. W., & Kuzio de Naray, R. 2010, *ApJ*, 717, L87
- Walsh, S. M., Jerjen, H., & Willman, B. 2007, *ApJ*, 662, L83
- Walsh, S. M., Willman, B., & Jerjen, H. 2009, *AJ*, 137, 450
- Whalen, D., O’Shea, B. W., Smidt, J., & Norman, M. L. 2008, *ApJ*, 679, 925
- Willman, B., et al. 2005a, *AJ*, 129, 2692
- Willman, B., et al. 2005b, *ApJ*, 626, L85
- Willman, B., Geha, M., Strader, J., Strigari, L. E., Simon, J. D., Kirby, E., & Warres, A. 2010, *ArXiv e-prints*
- Wise, J. H., & Abel, T. 2007, *ApJ*, 671, 1559
- Wise, J. H., & Abel, T. 2008, *ApJ*, 685, 40
- Wolf, J., Martinez, G. D., Bullock, J. S., Kaplinghat, M., Geha, M., Muñoz, R. R., Simon, J. D., & Avedo, F. F. 2010, *MNRAS*, 778
- Zentner, A. R., Kravtsov, A. V., Gnedin, O. Y., & Klypin, A. A. 2005, *ApJ*, 629, 219
- Zucker, D. B., et al. 2006a, *ApJ*, 650, L41
- Zucker, D. B., et al. 2006b, *ApJ*, 643, L103

|              | $R < 50$ kpc                    | $R > 50$ kpc  |
|--------------|---------------------------------|---|
| Inconsistent | Segue 1<br>Segue 2<br>Willman 1 | Pisces II<br>Leo V *  |
| Consistent   | Coma Ber.                       | Bootes I & II<br>CVn I & II<br>Hercules<br>Leo V & Leo T<br>Ursa Major I & II |

Table 3: Table of Milky Way ultra-faint dwarfs classified by their distance from our galaxy (columns) and whether or not they are consistent with our predictions for the fossils of the first galaxies (row). Note the correlation between distance and consistency. (\*) Pisces II and Leo V are both on the lower end of radii expected for fossils, as such they are marked as “inconsistent,” but are not as far from predictions as the “inconsistent” ultra-faints within 50 kpc.

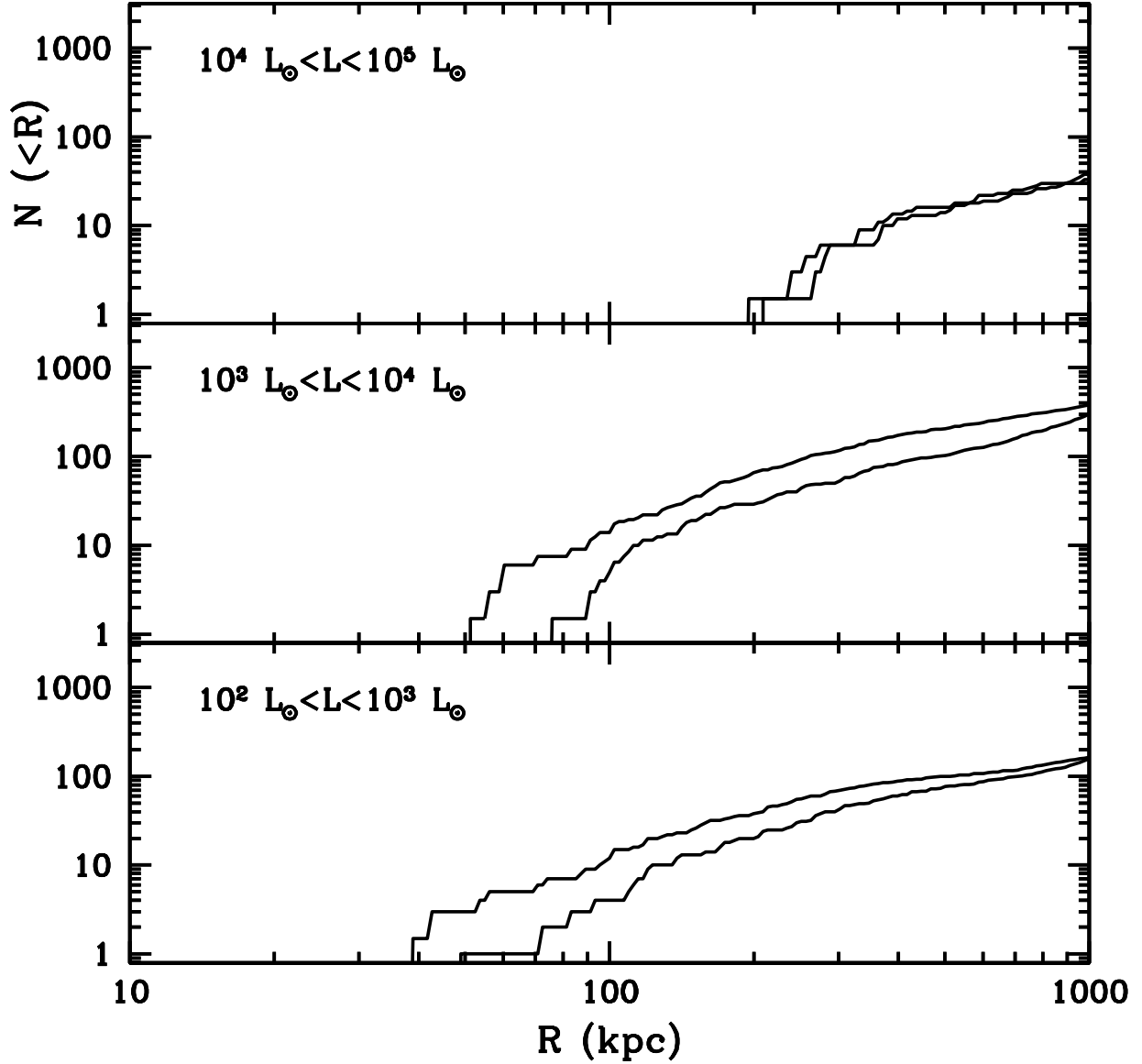


Fig. 3.— The galactocentric radial distribution of the fossils excluding the detectable dwarfs as determined by Walsh et al. (2009). Note that the bins have shifted down one order of magnitude in luminosity since there are no undetected fossils with  $L_V > 10^5 L_\odot$  and we have included the distribution for the lowest luminosity fossils with  $L_V < 10^3 L_\odot$ .

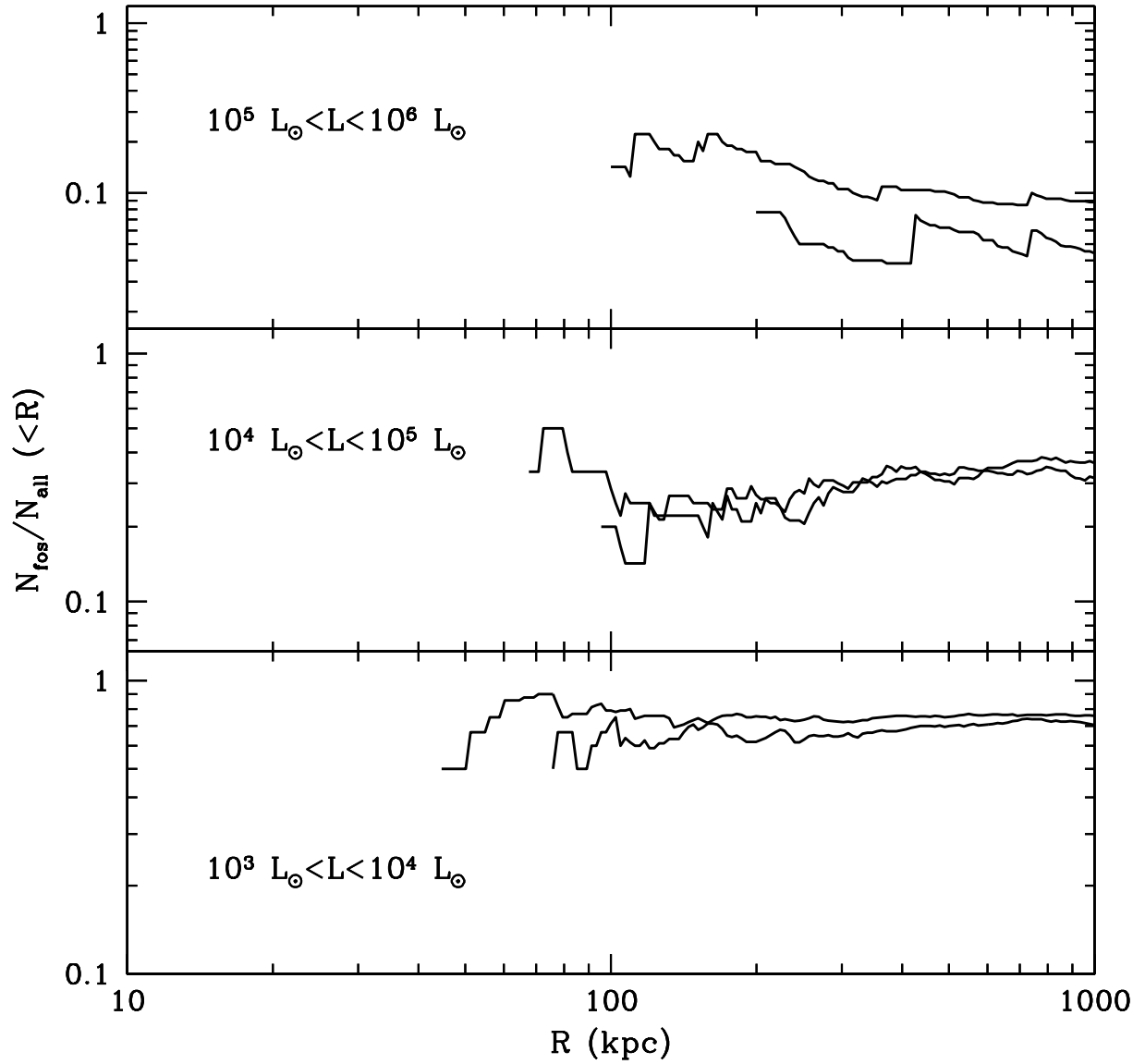


Fig. 4.— The galactocentric radial distribution of the fraction of luminous subhalos which are true fossils around MW.2 and MW.3 from Run D. They are divided in the luminosity bins from Figures 1 and 2 for which there is a fossil population ( $L_V < 10^6 L_{\odot}$ ).

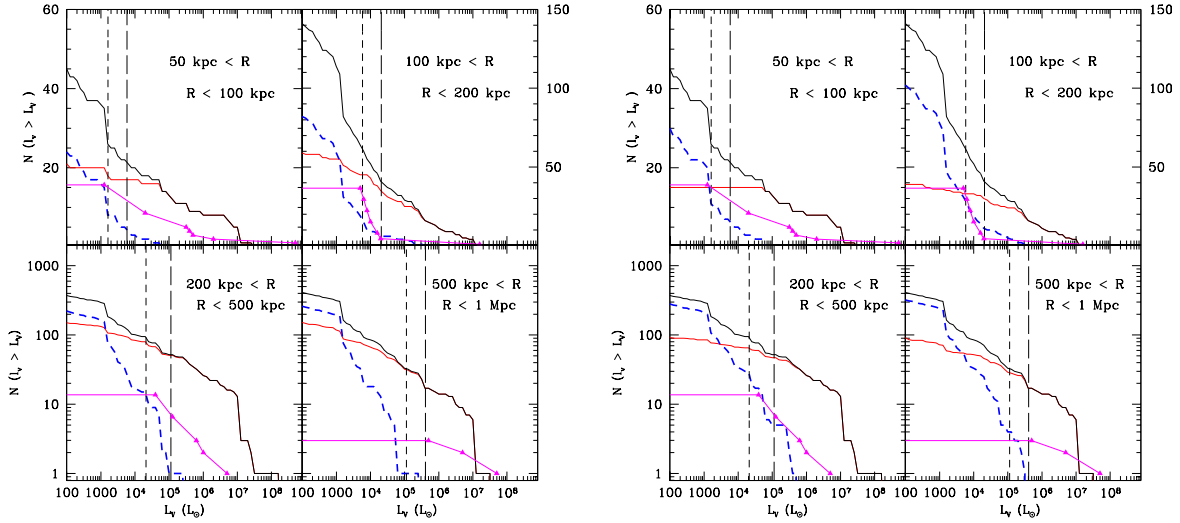


Fig. 5.— (*Left*). Cumulative primordial luminosity function of MW.3 from Run D with the observed luminosity function of Milky Way satellites. We have used a  $v_{filt} = 20 \text{ km s}^{-1}$  to determine whether a simulated halo is a non-fossil or true fossil. We show the luminosity functions for four distance bins,  $50 \text{ kpc} < R < 100 \text{ kpc}$  (upper left),  $100 \text{ kpc} < R < 200 \text{ kpc}$  (upper right),  $200 \text{ kpc} < R < 500 \text{ kpc}$  (lower left), and  $500 \text{ kpc} < R < 1 \text{ Mpc}$  (lower right). In all distance bins the relevant populations are noted as follows. The solid black curves show the total cumulative luminosity function from our simulations, the red solid lines shows the same for only the star forming halos (non-fossils, including polluted fossils). We show the true fossil population with the blue dashed curve. The total observed population is shown as magenta triangles with the ultra-faint dwarf distribution corrected for sky coverage of the SDSS. The detection limits given in Walsh et al. (2009) are shown as vertical black, dashed lines. Long dashed for the luminosity limit for the outer radii and shorter dashes for the inner radii in a given bin. (*Right*). Same as the figure on the left but for  $v_{filt} = 30 \text{ km s}^{-1}$ .



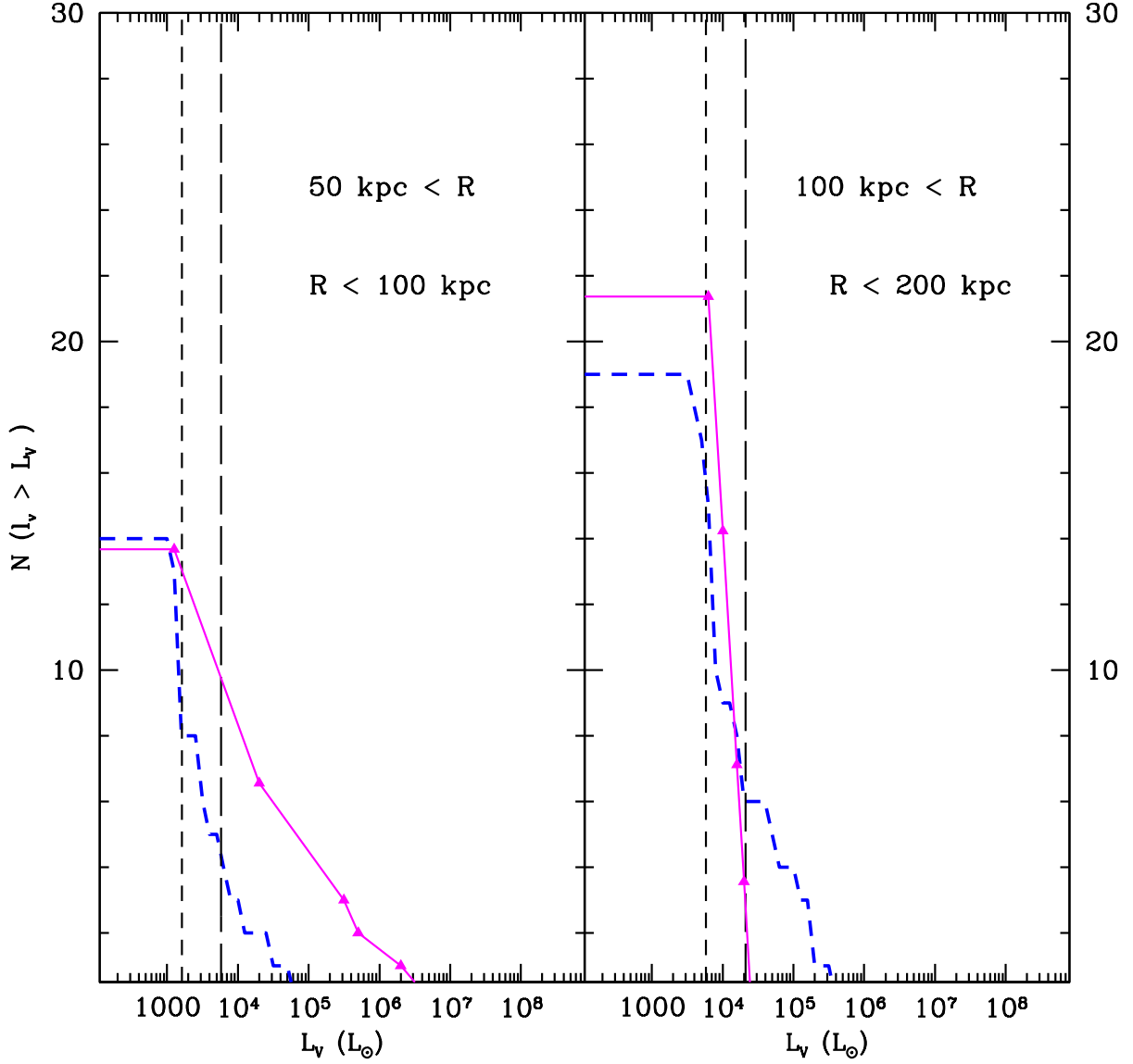


Fig. 6.— Cumulative primordial luminosity function for MW.3 in Run D and the total observed population with only the fossils plotted. The simulated fossils are shown as the blue dashed line and the observed fossils as the magenta triangles. The fossil criteria for the observed satellites is the same as in Figure 2. We have only shown subhalos around MW.3 which would be detectable by SDSS.

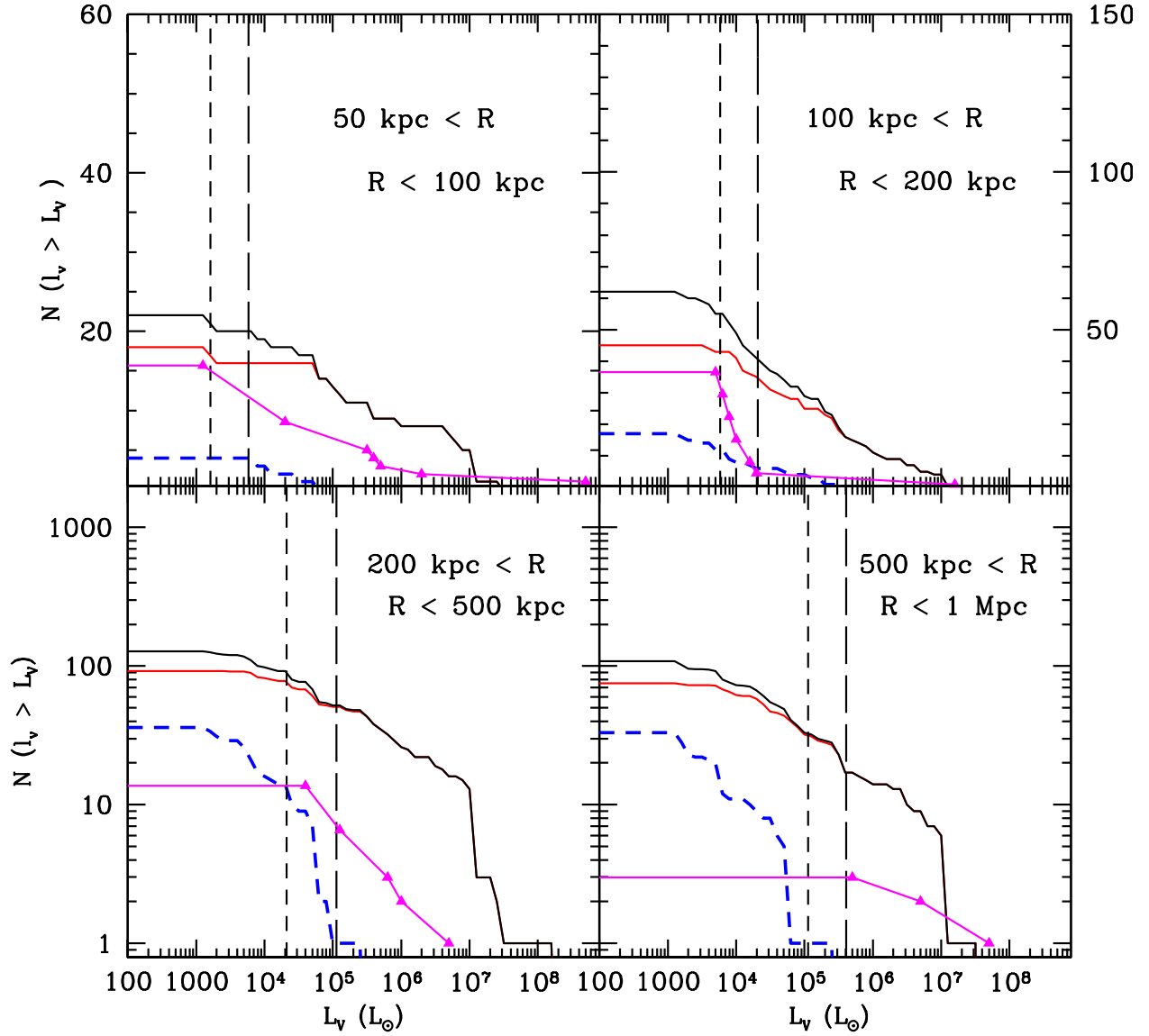


Fig. 7.— Cumulative primordial luminosity function for MW.3 in Run D and observations. Only simulated dwarfs which have  $\Sigma_V$  above the Koposov et al. (2008) limit are shown.

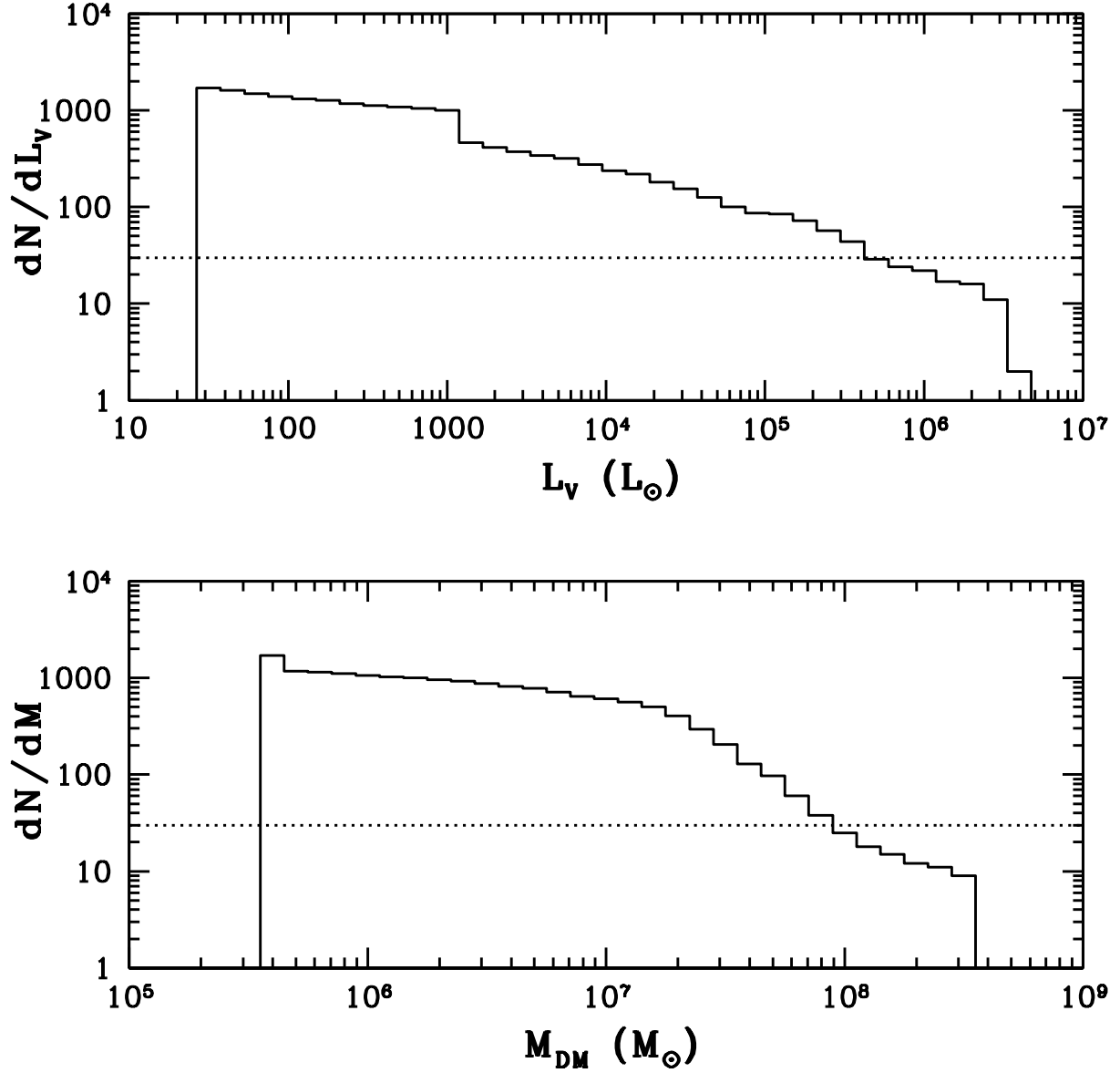


Fig. 8.— The luminosity (top) and mass (bottom) functions for pre-reionization halos within  $R_{vir}$  of MW.3 which are *not* part of a bound subhalo at  $z = 0$ . We only include those unbound luminous pre-reionization halos between 20 kpc and 50 kpc, where all but two of the known tidal ultra-faints are located. The horizontal dotted lines show the approximate number of stripped pre-reionization halos required to reproduce the inner ultra-faint population,  $\sim 30$ .

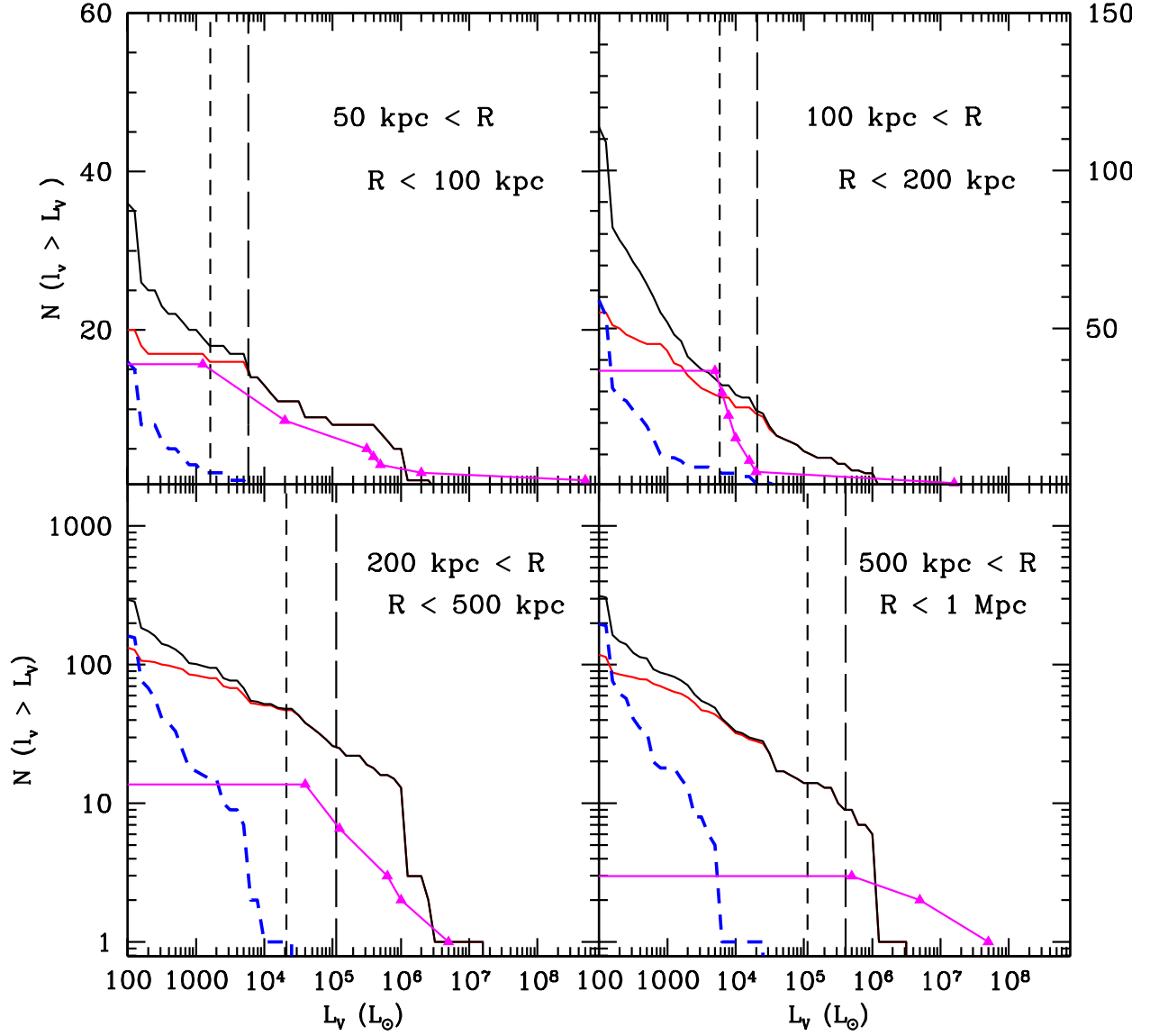


Fig. 9.— Cumulative luminosity functions of MW.3 from Run D (colored curves) with the total observed population (magenta triangles). All the symbols and lines mean the same as in Figure 5. Here we increase the stellar mass-to-light ratio by a factor of 10 to  $50 M_{\odot}/L_{\odot}$ .

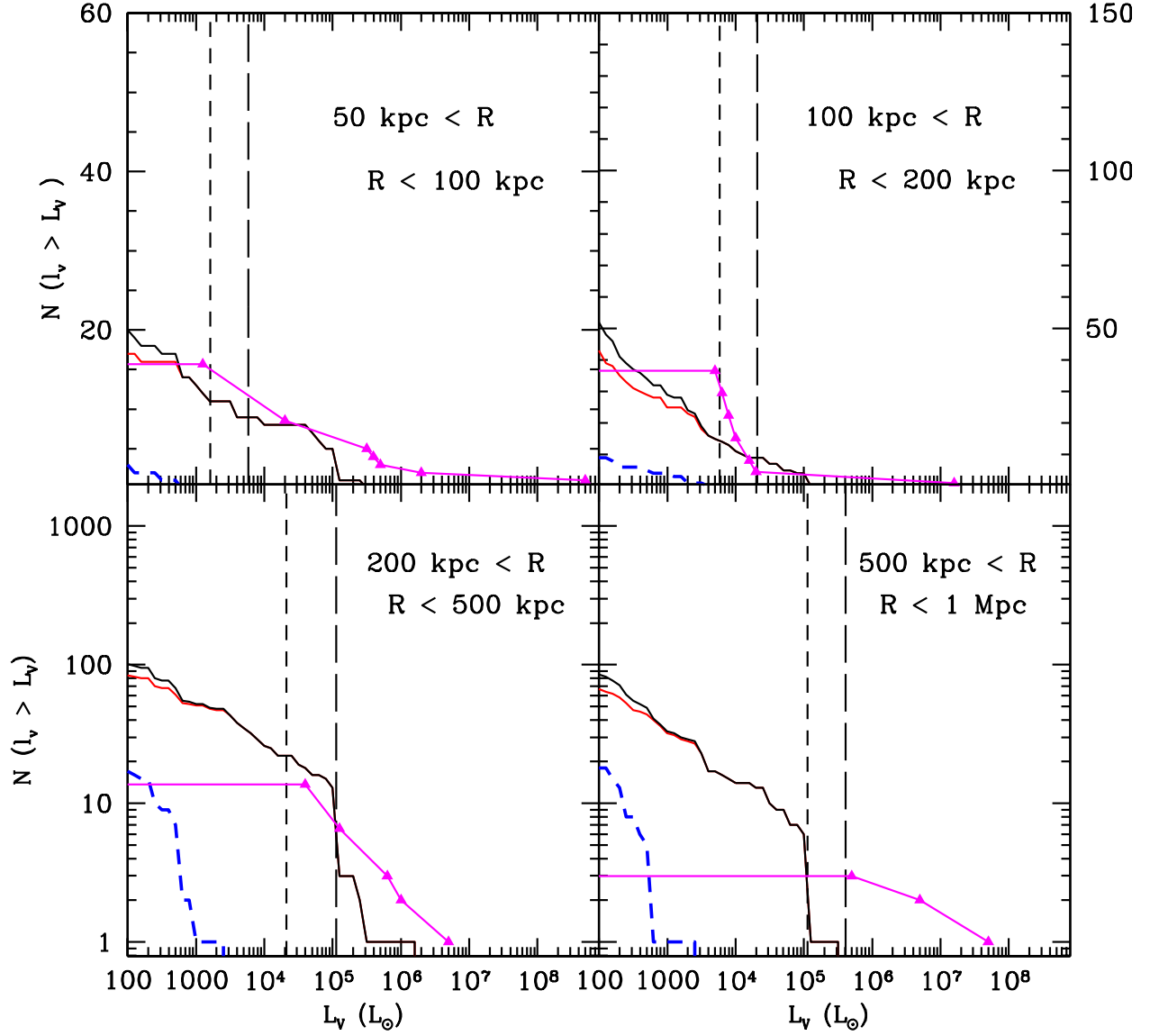


Fig. 10.— Cumulative luminosity functions of MW.3 from Run D (colored curves) with the total observed population (magenta triangles). All the symbols and lines mean the same as in Figure 5. Here we increase the stellar mass-to-light ratio by a factor of 100 to  $500 M_{\odot}/L_{\odot}$ .

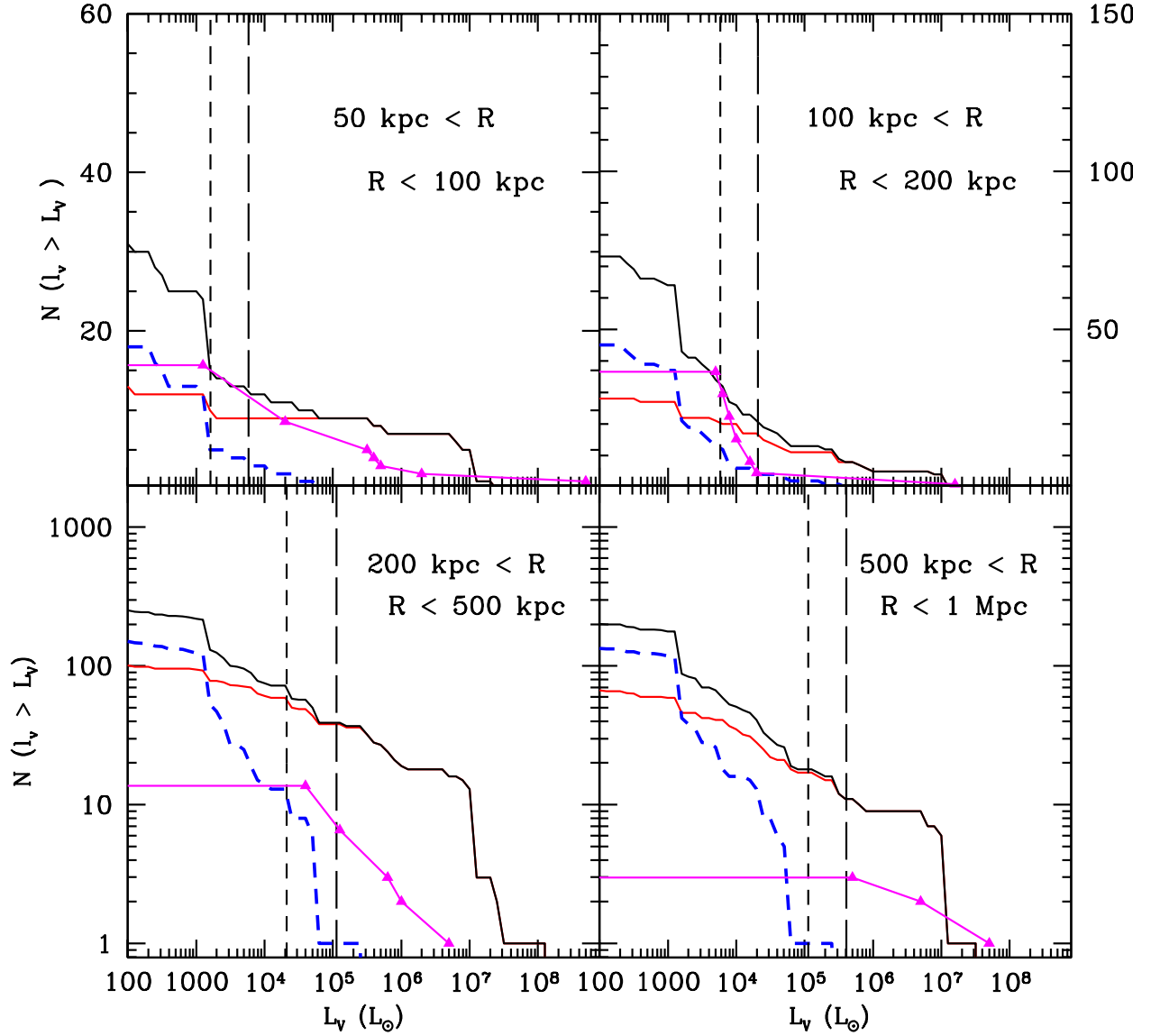


Fig. 11.— Cumulative luminosity functions of MW.3 from Run D (colored curves) with the total observed population (magenta triangles). All the symbols and lines mean the same as in Figure 5. Here we have completely suppressed star formation in any halo outside the highest density regions. This is the most extreme case of lower  $H_2$  formation, and therefore lower star formation in the voids.

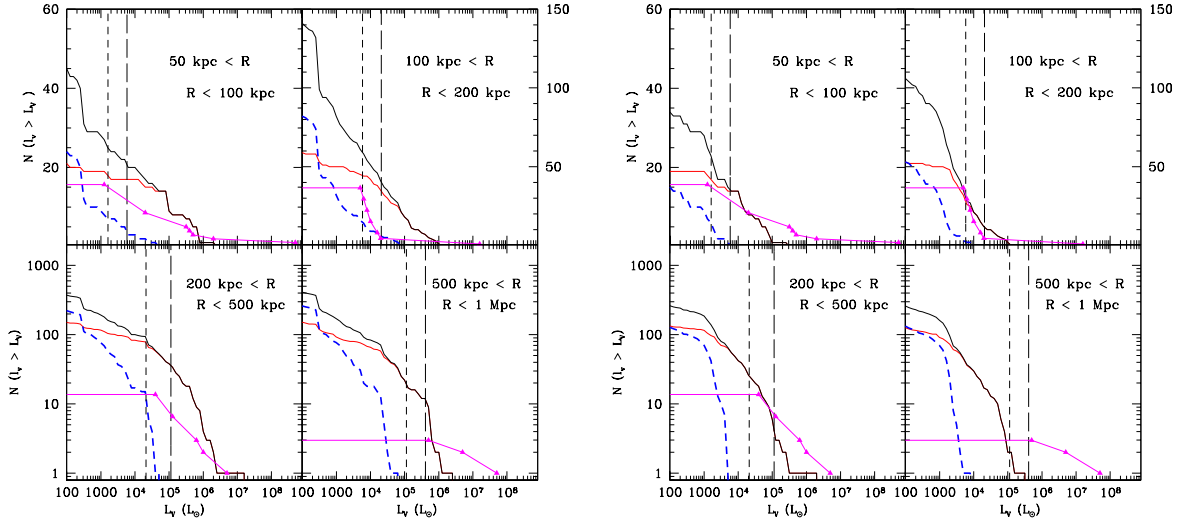


Fig. 12.— (*Left*). Cumulative luminosity function of MW.3 from Run D (colored curves) and the total observed population (magenta triangles). All symbols and lines mean the same as in Figure 5. We have applied an  $f_{crit} = 1\%$ . (*Right*). Same as left panel but for  $f_{crit} = 0.1\%$ .

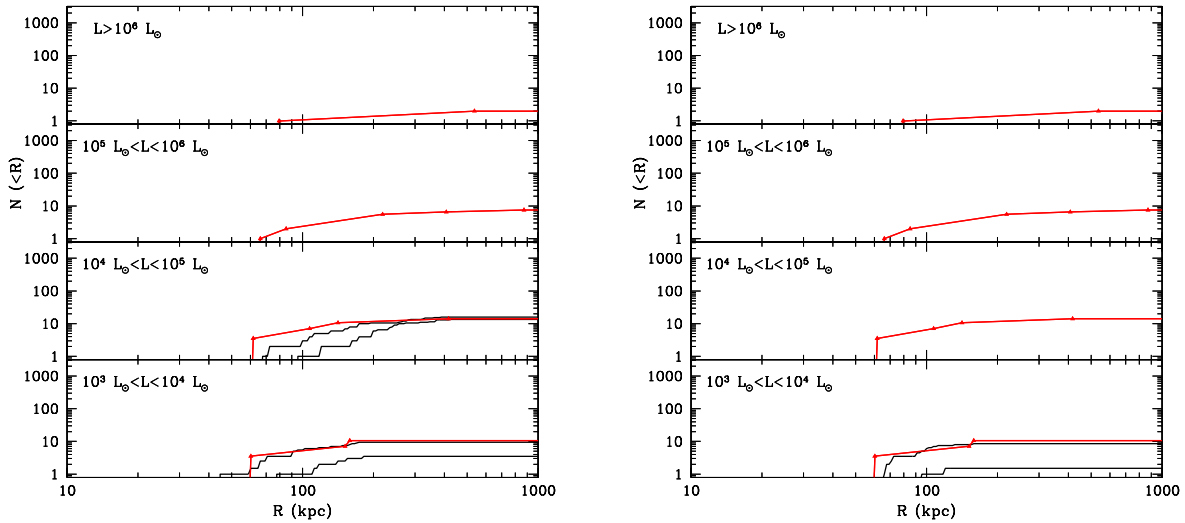


Fig. 13.— (*Left*) : Radial distribution for our simulated MW.2 and MW.3 with a  $f_{crit} = 1\%$  (black solid curves) and for the fossil Milky Way satellites (red triangles). Note, that while we are still able to reproduce the radial distribution of the lowest luminosity bin, we are no longer able to match the fossil population for  $L_V > 10^5 L_\odot$ . (*Right*) : Radial distribution for  $f_{crit} = 0.1\%$ . Note that for the more extreme suppression, we have lost the fossils population with  $L_V > 10^4 L_\odot$ .

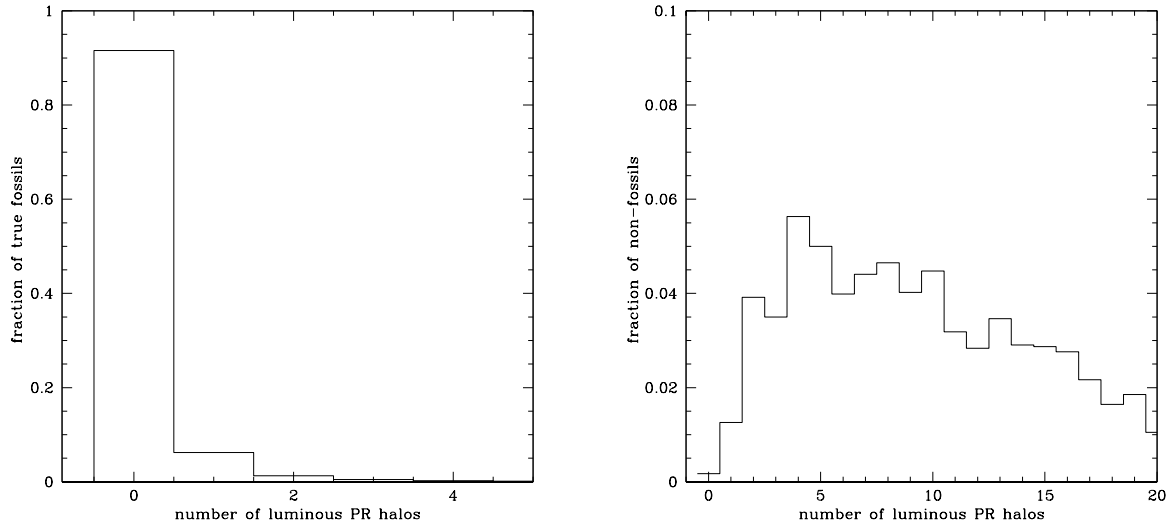


Fig. 14.— (*Left*). Histogram of the fraction of luminous true fossils with a given number of luminous pre-reionization halos,  $N_{lum}$ .  $N_{lum}$  is a proxy for the number of significant mergers the system has undergone. (*Right*). Histogram of the fraction of non-fossils with a given  $N_{lum}$ . Note, that unlike the  $N_{lum}$  histograms for the true fossils and polluted fossils the peak is not at  $N_{lum} = 0$ , but shifted to  $N_{lum} \sim 5$ . Note also, that the vertical scale is 0.1 instead of 1.0.



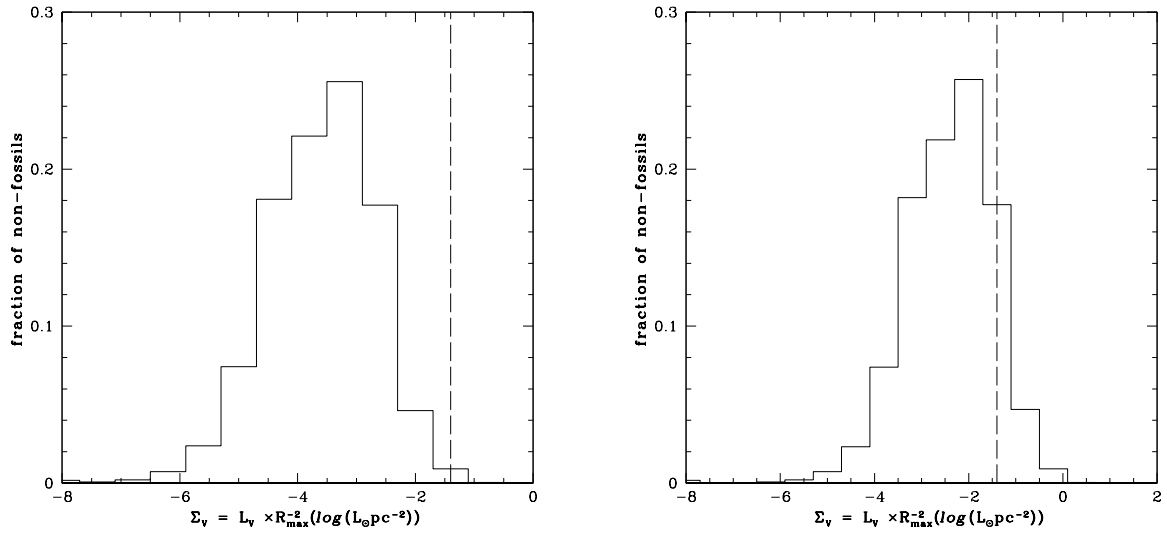


Fig. 15.— *(Left)* : Histogram of the fraction of non-fossils with a given V-band surface brightness,  $\Sigma_V$ , for the primordial population. We assume that the primordial stars have been puffed up by interactions until they fill the full extent of the dark matter halo, giving us  $\Sigma_V = L_V \times R_{max}^{-2}$ , where  $R_{max}$  is the radius at which  $v(r) = v_{max}$ . The dashed vertical line is the surface brightness limit of the SDSS from Koposov et al. (2008). Only  $\sim 1\%$  of the non-fossils are to the right of the dashed line, with expanded primordial populations detectable by the SDSS. *(Right)* : Histogram of the fraction of non-fossils with a given V-band surface brightness,  $\Sigma_V$ , for the primordial population. Here we assume that the ghost halo is more concentrated, extending only to  $0.25 \times R_{max}$ .

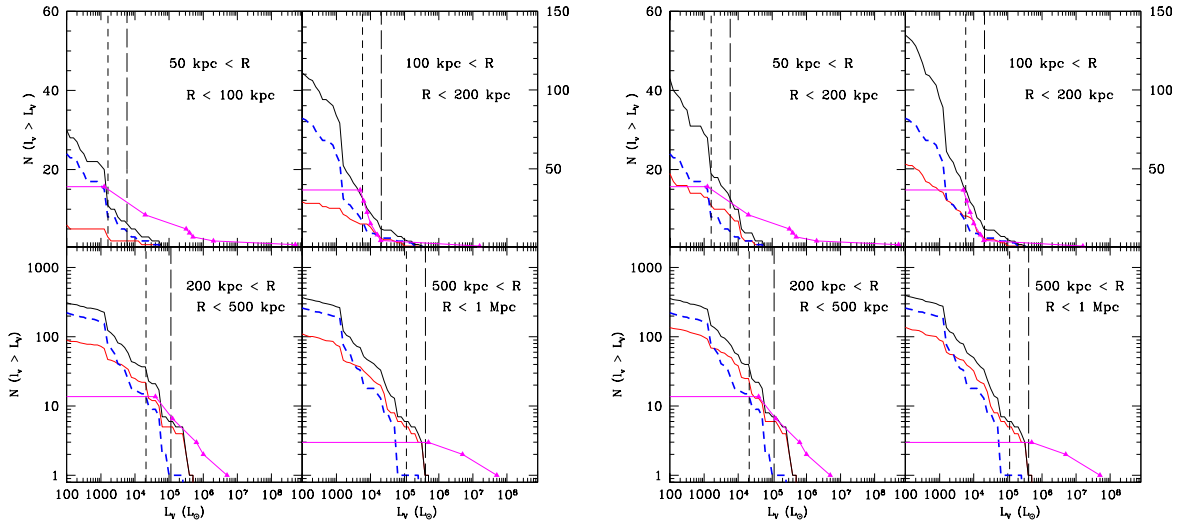


Fig. 16.— *Left* : Cumulative luminosity functions of MW.3 from Run D (colored curves) with the total observed population (magenta triangles). All the symbols and lines mean the same as in Figure 5. In this figure we assume that all the non-fossils are below the detection limits or have lost their entire stellar populations due to a combination of heating due to major mergers and tidal interactions. *Right* : Cumulative luminosity functions of MW.3 from Run D (colored curves) with observations (magenta triangles). All the symbols and lines mean the same as in Figure 5. Unlike Figure 16, here we allow the non-fossils to retain 0.1% of their stellar populations.